MiniBooNE Technical Note # 103 Version 1

The GEANT4-based beam Monte Carlo for MiniBooNE

Michel Sorel

October 21, 2003

Abstract

We describe the GEANT4 beam Monte Carlo program `BooNEG4Beam`, discuss the validation of the code, and present predictions for the ν_μ, $\bar{\nu}_\mu$, ν_e, $\bar{\nu}_e$ fluxes at the MiniBooNE detector.

Contents

1 Purpose of the Code

1.1 Main requirement: a flexible hadronic physics interface

The purpose of the MiniBooNE beam Monte Carlo is to predict the fluxes at the MiniBooNE detector for all relevant neutrino species (ν_μ, $\bar{\nu}_\mu$, ν_e, $\bar{\nu}_e$) as a function of neutrino energy, per proton on target and per unit area. The flux understanding is of primary importance for most MiniBooNE analyses, including for example neutrino cross-section meaurements, and $\nu_\mu \rightarrow \nu_e$ and $\nu_\mu \rightarrow \nu_{\not\mu}$ oscillation analyses.

As a consequence, a major effort is underway to refine the flux predictions by using (or planning to use) experimental information affecting these predictions, both from MiniBooNE data and from elsewhere:

1. compilation and reanalysis of existing pion and Kaon production data in proton-Beryllium interactions for proton beam momenta in the $\sim 10\ GeV/c$ range;
2. analysis of the BNL E910 data for $\pi^\pm,\ K^\pm,\ K^0$ production in $p + Be$ interactions at 6.0, 12.4, and 17.5 GeV/c proton beam momentum, on a thin Be target (5% λ_{inel});
3. analysis of the CERN HARP data for $\pi^\pm,\ K^\pm,\ K^0$ production in $p + Be$ interactions at 8.9 GeV/c beam momentum, on Be targets of various thicknesses (5%, 50%, 100% λ_{inel});
4. unfolding techniques to extract the neutrino fluxes from the observed rates in the MiniBooNE detector, assuming known neutrino cross-sections and no neutrino oscillations. For example, one proposed method is given in [1], and other methods are possible;
5. analysis of Little Muon Counters (LMC) data to constrain the ν_e flux in the detector due to $K^\pm$ decays.

It is important for MiniBooNE to have a beam Monte Carlo simulation program that makes use of the experimental information listed above, in order to:

1. get our best possible estimate for the neutrino fluxes as a function of energy;
2. assign well-defined overall uncertainties as well as neutrino energy bin-to-bin correlations for the neutrino fluxes.

The same type of approach, partially relying on information external to that of the neutrino detector itself, has been used successfully by other experiments, for example by the K2K [2] and NOMAD [3] experiments.

A single code with a flexible hadronic physics model interface is appealing in this respect: the user may wish to select which information on meson production in $p + Be$ interactions to use for estimating the neutrino fluxes and their associated uncertainty, without changing any other aspects of the simulation. The motivation for having a flexible hadronic physics interface is that the flux uncertainty is dominated by the secondary meson production uncertainty, and we can expect the many other physics processes (energy loss, multiple scattering, reinteractions, particle decay routines, etc.) and MiniBooNE-specific design issues (target region and decay volume geometry, transport in horn magnetic field, energy threshold for particles tracking, ntuple output format,

etc.) not to change as much in time as we refine our flux understanding.

Moreover, and most importantly, our understanding of the neutrino fluxes is likely to proceed by incremental steps, and a flexible framework for tuning the MiniBooNE particle production models in the target is desirable.

These goals can be accomplished in a variety of ways. Here we discuss one posible tool to implement these features, based on the MiniBooNE GEANT4 beam Monte Carlo, `BooNEG4Beam`. The generalization and abstraction of physics processes is a key issue in the design of Geant4 [4]. All physics processes are treated in the same manner from the tracking point of view. The GEANT4 approach enables the user to create a process (e.g. hadronic interactions in Beryllium) and assign it to a dynamic particle type (e.g. 8 GeV protons). This openness allows the creation of processes for novel, domain-specific or customised purposes by users (e.g. a "HARP" physics process). The custom-defined physics models are defined in the initialization phase, and no reweighting procedure at the tracking level is necessary to match the desired production cross-sections.

1.2 Additional requirements

Apart from the flexibility in selecting a hadronic physics model for particle production in proton-Beryllium interactions, specific requirements for the MiniBooNE beam simulation tools are:

beamline geometry: capability to change the geometry specifications of the simulation, for example switching from a 50m to a 25m long MiniBooNE decay region, HARP production measurements geometries;

event generator: capability to change the transverse spot size and beam divergence of the Booster primary proton beam incident on the MiniBooNE target;

horn magnetic field: capability to change the MiniBooNE horn magnetic field;

particle biasing techniques: capability to boost the statistics on certain neutrino types at the MiniBooNE detector (e.g. ν_e's from Kaons), and therefore reduce the statistical uncertainty associated with the Monte Carlo simulation, by "sampling" more frequently certain particle types;

output: capability to store particle information, depending on their type (e.g. neutrinos), momentum, parent momentum, direction, in a form suitable for other MiniBooNE software tools.

The above list is not meant to be complete, but rather represent some of the current user interface commands that the user can execute within the execution of a G4 beam Monte Carlo simulation, in addition to the built-in G4 user interface commands. The structure of the GEANT4 kernel and the MiniBooNE GEANT4 application `BooNEG4Beam`, together with their available user interface commands, are given in Section2.

2 Code structure and functionality

2.1 GEANT4 class categories

Readers who are familiar with the GEANT3 code structure and functionality can skip this section.

From the GEANT4 "User's Guide: For Application Developers", [4]:

"Geant4 is a free software package composed of tools which can be used to accurately simulate the passage of particles through matter. Geant4 is written in C++, and consists of about one million lines of code and about one thousand classes. Aspects of the simulation process included in Geant4 are:

- *the geometry of the system,*
- *the materials involved,*
- *the fundamental particles of interest,*
- *the generation of primary events,*
- *the tracking of particles through materials and electromagnetic fields,*
- *the physics processes governing particle interactions,*
- *the response of sensitive detector components,*
- *the generation of event data,*
- *the storage of events and tracks,*
- *the visualization of the detector and particle trajectories, and*
- *the capture and analysis of simulation data at different levels of detail and refinement.*

Users may construct stand-alone applications or applications built upon another object-oriented framework. In either case the toolkit will support them from the initial problem definition to the production of results and graphics for publication. To this end, the toolkit includes:

- *user interfaces,*
- *built-in steering routines, and*
- *command interpreters*

which operate at every level of the simulation.

The class category diagram designed for Geant4 is shown in the figure below. Each class category is represented by a box in the figure, and a "uses" relation by a straight line. The circle at an end of a straight line means the class category which has this circle uses the other category. A class category is a "cluster of [C++] classes that are themselves cohesive, but are loosely coupled relative to other clusters".

The following is a brief summary of the role of each class category in Geant4.

1. *Run and Event*
   These are categories related to the generation of events, interfaces to event generators, and any secondary particles produced. Their roles are principally to provide particles to be tracked to the Tracking Management.

2. *Tracking and Track*
   These are categories related to propagating a particle by analyzing the factors limiting the step and applying the relevant physics processes. The important aspect of the design was that a generalized Geant4 physics process (or interaction) could perform actions, along a tracking step, either localized in space, or in time, or distributed in space and time (and all the possible combinations that could be built from these cases).

3. *Geometry, Magnetic Field and CAD-Interface*
   These three categories manage the geometrical definition of a detector (solid modeling and interactions with CAD systems) and the computation of distances to solids (also in a magnetic field). The Geant4 geometry solid modeler is based on the ISO STEP standard and it is fully compliant with it, in order to be able to exchange geometrical information with CAD systems. A key feature of the Geant4 geometry is that the volume definitions are independent of the solid representation. By this abstract interface for the G4 solids, the tracking component works identically for various representations. The treatment of the propagation in the presence of fields has been provided within specified accuracy. An OO design allows us to exchange different numerical algorithms and/or different fields (not only B-field), without affecting any other component of the toolkit

4. *Particle Definition and Matter*
   These two categories manage the the definition of materials and particles.

5. *Physics*
   This category manages all physics processes participating in the interactions of particles in matter. The abstract interface of physics processes allows multiple implementations of physics models per interaction or per channel. Models can be selected by energy range, particle type, material, etc. Data encapsulation and polymorphism make it possible to give transparent access to the cross sections (independently of the choice of reading from an ascii file, or of interpolating from a tabulated set, or of computing analytically from a formula). Electromagnetic and hadronic physics were handled in a uniform way in such a design, opening up the physics to the users.

6. *Hits and Digitization*
   These two categories manage the creation of hits and their use for the digitization phase. The basic design and implementation of the Hits and Digi had been realized, and also several prototypes, test cases and scenarios had been developed before the alpha-release. Volumes (not necessarily the ones used by the tracking) are aggregated in sensitive detectors, while hits collections represent the logical read out of the detector. Different ways of creating and managing hits collections had been delivered and tested, notably for both single hits and calorimetry hits types. In all cases, hits collections had been successfully stored into and retrieved from an Object Data Base Management System.

7. *Visualization*
   This manages the visualization of solids, trajectories and hits, and interacts with underlying

graphical libraries (the Visualization class category). The basic and most frequently used graphics functionality had been implemented already by the alpha-release. The OO design of the visualization component allowed us to develop several drivers independently, such as for OpenGL and OpenInventor (for X11 and Windows), DAWN, Postscript (via DAWN) and VRML.

8. *Interfaces*
   This category handles the production of the graphical user interface (GUI) and the interactions with external software (OODBMS, reconstruction etc.).”

2.2 MiniBooNE-specific classes

The MiniBooNE GEANT4 application `BooNEG4Beam`, available in CVS, currently consists of:

1. `BooNEG4Beam.cc`, containing the main method of the application;
2. `jobOptions.in`, where user interface commands are specified (the user can change the name of this file);
3. utility scripts to set the G4 environment and to run G4 batch jobs;
4. libraries for each of the geometry specifications, in the `geometry/` subdirectory. Currently there are five geometry specifications, two for the MiniBooNE beamline (with and without a 25m absorber), three for MiniBooNE target geometries used in the HARP experiment at CERN;
5. libraries for each of the physics models available for inelastic interactions of primary protons in Beryllium, in the `physics/` subdirectory. Currently there are four physics models available;
6. 25 classes contained in the `src/` and `include/` subdirectories, representing the “meat” of the program.

A brief description of the 25 `BooNEG4Beam` classes follows. We start from some naming conventions:

1. filenames starting with `BooNE` refer to classes that have been specifically written or modified for the MiniBooNE beam Monte Carlo;
2. filenames starting with `ExN` refer to classes copied from GEANT4 novice examples classes of the current G4 distribution;
3. filenames ending in `Action` refer to user action classes. All objects of user action classes are registered with `G4RunManager`;
4. filenames ending in `Messenger` refer to `G4UImessenger` derived classes providing the MiniBooNE-specific interface commands available to the user in the `jobOptions.in` file. The availability of individual user interface commands, the ranges of parameters, the available candidates on individual command parameters may vary dynamically during the execution of the beam Monte Carlo job. All objects of messenger classes are instantiated in the respective user action class: for example, `BooNEPrimaryGeneratorActionMessenger` is instantiated in `BooNEPrimaryGeneratorAction`. For a complete list of all user interface commands available in `BooNEG4Beam`, the reader should consult the GEANT4 MiniBooNE web page, located at [5].

The MiniBooNE-specific classes can be subdivided according to the same class category given in the previous subsection. For more details on the software aspects of the simulation, the reader should consult the "Software Reference Manual" at [4], where most GEANT4 class header files can be browsed.

1. Run and Event

   i. `BooNERunAction`: inherits from the `G4UserRunAction` virtual class. Defines user actions at the run level of the simulation. The `BeginOfRunAction` and `EndOfRunAction` methods are used to communicate with the `RecorderBase` and `BooNEOutput` interface classes (see the "Interfaces" list later on in this section) to book and to write to file the ntuples with the results of the simulation for that particular run.

   ii. `BooNEEventAction`: inherits from the `G4UserEventAction` virtual class. Defines user actions at the event level of the simulation. The `RecordEndOfEvent` method is used to communicate with the `RecorderBase` and `BooNEOutput` classes to fill the ntuples information with selected trajectories.

   iii. `ExN03EventActionMessenger`: inherits from the `G4UImessenger` class and is instantiated in `BooNEEventAction`. Defines the event level user interface commands.

   iv. `BooNEPrimaryGeneratorAction`: inherits from the `G4VUserPrimaryGeneratorAction` virtual class. Defines user actions at the event generator level of the simulation. The `GeneratePrimaries` method describes how initial particles are to be generated, in this case 8 GeV protons.

   v. `BooNEPrimaryGeneratorActionMessenger`: defines the interface commands available to the user at the event generator level. In particular, the parameters setting the gaussian position and angular widths of the proton beam in both transverse directions (x, y) are implemented in this class.

2. Tracking and Track

   vi. `BooNETrackingAction`: inherits from the `G4UserTrackingAction` virtual class. Defines user actions at the track level of the simulation. The `PreUserTrackingAction` and `PostUserTrackingAction` methods are used to copy track information at track's creation and destruction into the `BooNETrajectory` object (see `BooNETrajectory` description), for tracks that are relevant for the MiniBooNE neutrino fluxes predictions. Moreover, particle biasing techniques are implemented in this class, following the prescription first suggested by Byron Roe [6]. The motivation for particle biasing techniques in the MiniBooNE beam Monte Carlo is to allow the user to boost the statistics for intirnsic ν_e's in the beam while minimizing the impact on the CPU time of the simulation.

   vii. `BooNETrackingActionMessenger`: defines the user interface commands available at track level. In particular, the user interface commands to select particle biasing techniques are defined in this class.

   viii. `BooNETrajectory`: inherits from the `G4VTrajectory` virtual class and is instantiated in `BooNETrackingAction`. This class represents the trajectory of a tracked particle, and contains the list of trajectory points which compose the trajectory, static (e.g. charge, mass, etc.) as well as dynamic (e.g. momentum, position, etc.) information of the track, and the identifier of its parent trajectory. Most of this information is taken from the

G4Ttrack class. This class is needed for two reasons: first, G4Track objects are transient objects, and do not exist in memory anymore by the time the end of the event is reached, when the ntuple is being filled; second, the BooNETrajectory class makes it possible to select tracks based on the parent track information. BooNETrajectory makes tracks persistent until the end of an event, and stores all the information needed by the beam Monte Carlo.

ix. BooNESteppingAction: inherits from the G4UserSteppingAction virtual class. Defines user actions at the step level of the simulation. In particular, tracks which are not relevant for the MiniBooNE neutrino fluxes predictions are killed, and optional ntuples with extra track information can be filled by this class, for debugging purposes.

3. Geometry, Magnetic Field and CAD-Interface

x. BooNEGeometryConstruction: inherits from the G4VUserDetectorConstruction class and is registered with G4RunManager. Defines the geometry of the simulation: volumes, volume attributes such as the horn magnetic field, and materials. With the exception of the magnetic field, all "geometry" specifications are automatically converted from the corresponding GEANT3.21 geometries, using the call list interpreter G4BuildGeom.cc of the G3toG4 facility.

xi. BooNEGeometryConstructionMessenger: defines the user interface command specifying the geometry call list filename.

xii. BooNELocalField: inherits from the G4MagneticField class and is instantiated in BooNEGeometryConstruction. For the MiniBooNE geometry files, defines a local, non-uniform magnetic field within the horn volume (via the GetFieldValue method), and defines various options for integrating the equation of motion of the particle in that field.

xiii. BooNELocalFieldMessenger: defines the user interface command specifying the horn electric current.

4. Particle Definition and Matter: none

5. Physics

xiv. BooNEPhysicsList: inherits from the G4VModularPhysics virtual class and is instantiated in the main method of the simulation. This is the top-level class for constructing particles and physics processes. The classes describing the general, electromagnetic, muon, hadron, and ion physics are registered to the process manager in BooNEPhysicsList.

xv. BooNEHadronPhysics: inherits from the G4VPhysicsConstructor virtual class and is instantiated in BooNEPhysicsList. Constructs all mesons, baryons, resonances and quarks, and physics processes specific to these particles.

xvi. BooNEpBeInteraction: inherits from the G4HadronicInteraction class and is instantiated in BooNEHadronPhysics. Defines secondary particle production (particle types, multiplicities, momenta) for inelastic interactions of primary protons in Beryllium.

xvii. BooNEpBeInteractionMessenger: defines the user interface commands specifying the physics model to be used for inelastic interactions of primary protons in Beryllium.

xviii. ExN04EMPhysics: inherits from the G4VPhysicsConstructor virtual class and is instantiated in BooNEPhysicsList. Constructs photons, electrons and neutrinos, and physics processes specific to these particles.

xix. `ExN04GeneralPhysics`: inherits from the `G4VPhysicsConstructor` virtual class and is instantiated in `BooNEPhysicsList`. Defines particle decays.

xx. `ExN04IonPhysics`: inherits from the `G4VPhysicsConstructor` virtual class and is instantiated in `BooNEPhysicsList`. Defines nuclei and light ions (e.g.deuterons, etc.), and physics processes specific to these particles.

xxi. `ExN04MuonPhysics`: inherits from the `G4VPhysicsConstructor` virtual class and is instantiated in `BooNEPhysicsList`. Defines muons and tau leptons, and physics processes specific to these particles.

6. Hits and Digitization: none

7. Visualization

xxii. `ExN02VisManager`: inherits from the `G4VisManager` virtual class and is instantiated in the `main` method of the simulation. Defines the graphics systems to be used for geometry and tracks visualization via the `RegisterGraphicsSystems` method. Exploits C-pre-processor variables (e.g `G4VIS_USE_DAWN`, etc.) which are set by the GNUmakefiles if the environment variables of the same name are set. Several graphics systems are registered and available in `BooNEG4Beam`; the only one tested (and working very nicely) is `VRML2FILE`, creating GEANT4 scenes in VRML formats (version 2). Several VRML browsers for Linux can be downloaded for free (e.g. `http://www.sim.no`).

8. Interfaces

xxiii. `RecorderBase`: this is a virtual base class used for storing information about the simulation at all levels (run, event, etc.). This class was originally written by Bill Seligman for the G4 simulation of the ATLAS electromagnetic barrel calorimeter.

xxiv. `BooNEOutput`: inherits from the `RecorderBase` class and is instantiated in the `main` method of the simulation. This class stores track and parent track information for selected tracks into HBOOK ntuples. In addition, the muon polarization vector in its rest frame is calculated, as done in the GEANT3 MiniBooNE beam Monte Carlo by Geoff Mills. `BooNEOutput` uses `cfortran` to bridge the FORTRAN HBOOK and CERNLIB codes to the GEANT4 C++ code.

xxv. `BooNEOutputMessenger`: defines the user interface commands specifying the options for the simulation output: which ntuples should be written, and with which kinematic selection on tracks and parent tracks.

2.3 How to build and run the simulation

The five steps below contain brief, practical explanations on how to get the source code, setup the GEANT4 environment, compile, run, and interpret the output of a `BOONEG4Beam` simulation. This paragraph is extracted from the `BooNEG4Beam README` file in CVS.

STEP 1 : get the source code

1. If the user already has an existing version of `BooNEG4Beam`, then he/she should `cd` to the existing BooNEG4Beam directory, and type:
   `cvs update`

2. If not, the user should type:
   `cvs checkout -d BooNEG4Beam miniboone/BooNEG4Beam`
   to get a local copy of `BooNEG4Beam` into the `BooNEG4Beam/` subdirectory, created in the directory where the cvs command was issued.

STEP 2 : setup the GEANT4 environment

```
cd BooNEG4Beam
source setup.env
```

This will set G4 environment variables, such as $G4INSTALL, $G4WORKDIR, etc.. In order to have a user's work directory that is different from the current one, the user should edit the "`setenv G4WORKDIR $PWD`" line in `setup.env`

STEP 3 : compile the code

```
gmake
```

Depending on the compilation options, many warnings might appear (mostly due to the `cfortran` package), but hopefully no errors. As is, the code works on the Linux platform only.

STEP 4 : run

There is only one executable for batch or interactive mode, and for non-visualization or visualization mode.

1. Batch mode
   In the `BooNEG4Beam/` subdirectory, there is a macro file template, containing the batch job options, called `jobOptions.in`. This is meant as a template, and the user should modify it as he/she wishes. For a list of all built-in and MiniBooNE-specific commands available as job options, the reader should refer to the GEANT4 documentation web page [4], and to the MiniBooNE G4 beam Monte Carlo web page [5]. To run in batch mode on a local machine, the user should issue the commands:
   ```
   source ./setup.env
   $G4WORKDIR/bin/$G4SYSTEM/BooNEG4Beam jobOptions.in
   ```
   There is nothing special with the name `jobOptions.in`, and the user can rename it. Most of the commands in the macro file are self-explanatory.
2. Batch mode using Condor
   When submitting G4 jobs on Condor, the user needs to specify the G4 environment for the target machine picked up by Condor. This means sourcing the `setup.env` file on the target machine. The user should execute the short script `BooNEG4Beam_wrapper.csh` in CVS, rather than `BooNEG4Beam`:
   ```
   boone-jobsub -M ./BooNEG4Beam_wrapper.csh
   ```
   and NOT:
   ```
   boone-jobsub $G4WORKDIR/bin/$G4SYSTEM/BooNEG4Beam jobOptions.in
   ```
   This wrapper script for CONDOR job execution is provided to show the simplest possible template wrapper; more sophisticated wrappers can be created, following the specifications given in [7].
   Note on visualization: some more work needs to be spent on visualization. For now, the VRML2FILE driver is the recommended one. At run completion, a new file named `g4_01.wrl` (or similar) should be created, which is be readable with a VRML 2 viewer. A VRML viewer for Linux (`VRMLview`) can be downloaded from `http://www.sim.no`.

3. Interactive mode
   To run in interactive mode, the user should issue the command:
   `$G4WORKDIR/bin/$G4SYSTEM/BooNEG4Beam`
   and then subsequent commands as he/she wishes. The command syntax should be the same the same as in the `jobOptions.in` file. It is possible to navigate into user interface command directories (e.g. `cd`, `ls`, etc.) as in UNIX.

STEP 5 : interpret the output of your simulation

By default, only ntuple 1000 is stored in the HBOOK file specified by the command `/boone/output/hbookFile`. Optionally, ntuples 2000, 3000 and 4000 are stored in the same HBOOK file. To find out what information is stored in these ntuples, see [5].

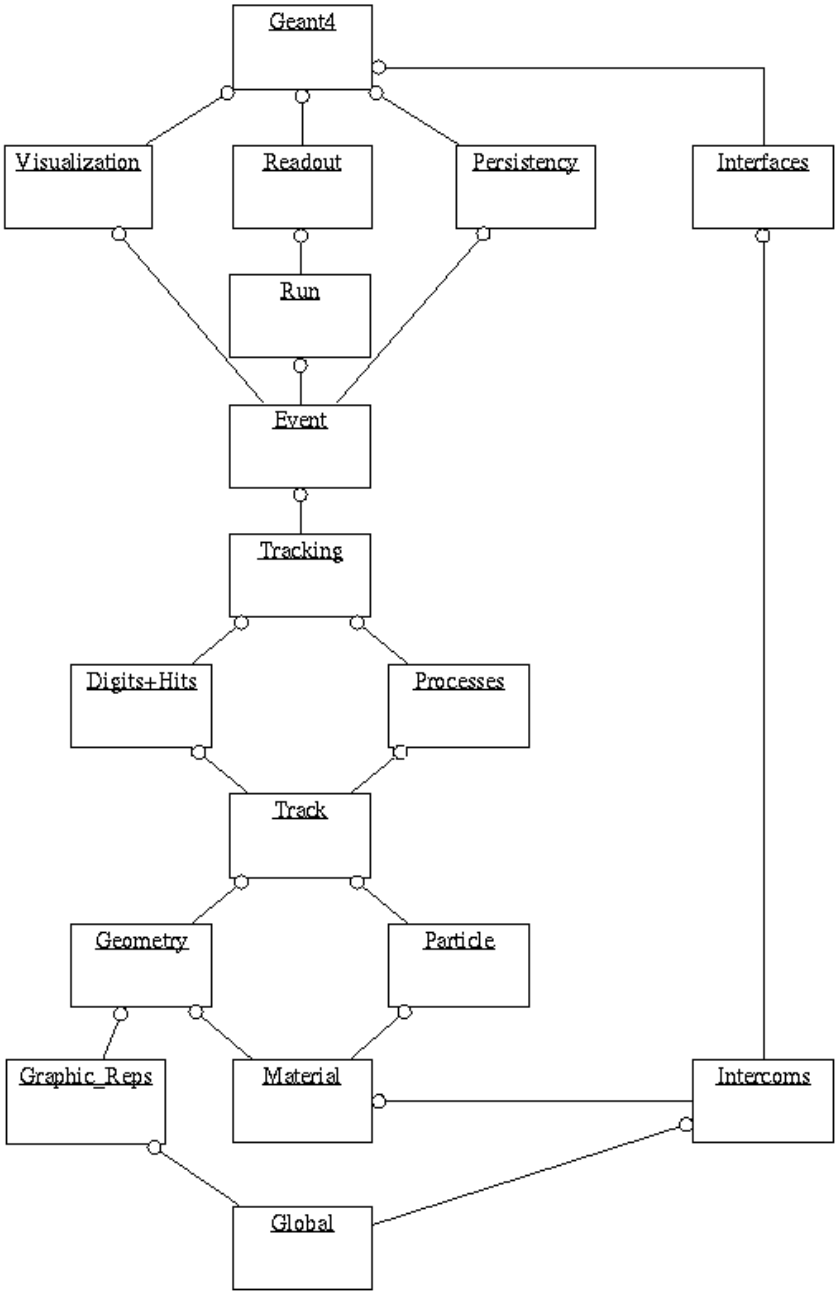

Figure 1: GEANT4 class categories. Eaich box represents a class category. The circle at the end of a straight line means that the class category which has this circle uses the other line-connected category.

3 Code validation 1: geometry and event generator

In this Section we discuss the concrete implementation in `BooNEG4Beam` of two mandatory G4 user action classes: the geometry construction and primary generator classes.

3.1 Geometry

As far as geometry and materials definitions are concerned, `BooNEG4Beam` reuses the work done for the GEANT3.21 beam Monte Carlo, `BooBeamMC`, by automatically converting G3 geometries and materials into G4 via the `G3toG4` facility in G4. Therefore, no coding of geometry specifications in G4 has been necessary. The automatic conversion is done in three steps:

G3→RZ : run the G3 beam Monte Carlo in interactive mode (i.e. run the `gxint` executable), to convert the MiniBooNE geometry data structure specified in the G3 cardfile into an RZ file;

RZ→ASCII : once the RZ file is available, it can be converted into an ASCII call list file by running the `rztog4` GEANT4 utility. This ASCII file contains the instructions on how to build the geometry. Examples of such files, which are human-readable and reflect the G3 syntax, can be found in the `geometry/` subdirectory of `BooNEG4Beam`. The source code of `rztog4` is FORTRAN;

ASCII→G4 : the call list interpreter `G4BuildGeom.cc`, called in `BooNEGeometryConstruction.cc` and defined in `$G4INSTALL/source/g3tog4`, read the instructions in ASCII format and builds the geometry in the G4 code.

For consistency, all geometry specifications in `BooNEG4Beam` are given in the form of an ASCII call list file. In the `geometry/` subdirectory, there are currently five possible choices of geometries and materials specifications:

1. `BooNE_50m.geom`: MiniBooNE geometry with a 50 m long decay region;
2. `BooNE_25m.geom`: MiniBooNE geometry with a 25 m long decay region;
3. `HarpTarget_5.geom`: Be target and support structure for the 5% λ_{inel} Be target used during the data-taking in the HARP detector in summer 2002 (λ_{inel} refers to the inelastic interaction length);
4. `HarpTarget_50.geom`: Be target and support structure for the 50% λ_{inel} Be target used in HARP. This target is made of two out of the seven 25% λ_{inel} Be slugs currently used in the MiniBooNE beamline;
5. `HarpTarget_100.geom`: Be target and support structure for the 100% λ_{inel} Be target used in HARP. This target is made of four out of the seven 25% λ_{inel} Be slugs currently used in the MiniBooNE beamline.

For the three HARP targets, the geometry specifications were already given in ASCII format, and the G3→RZ→ASCII conversion was not necessary.

In Fig.2, four images of the `BooNE_50m.geom` geometry are shown. The images show the entire decay region, and details of the target pile region, horn, and target. These images are produced

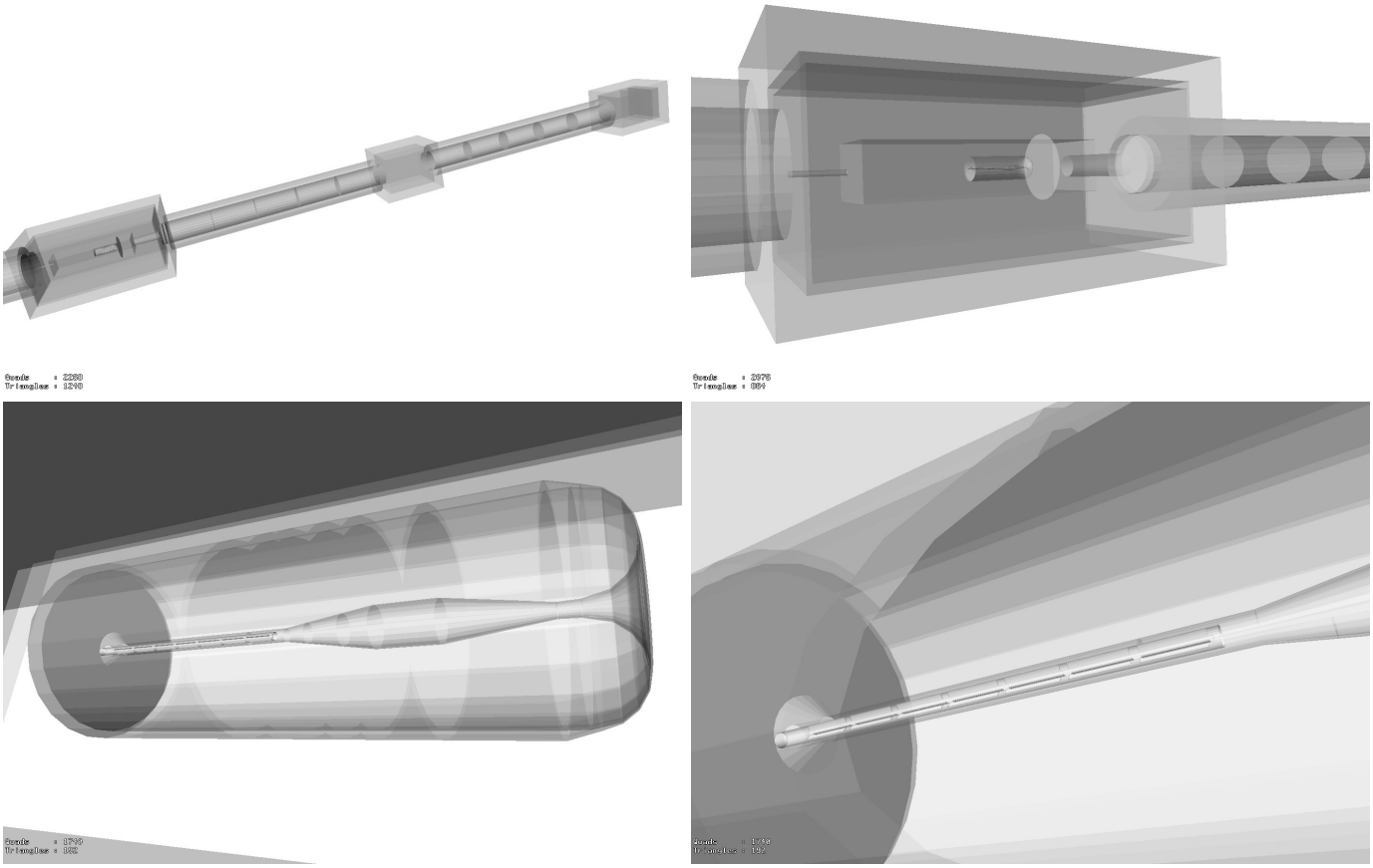

Figure 2: Snapshots of the MiniBooNE geometry implemented in the beam Monte Carlo. Pictures refer to the 50 m long decay region configuration. From the top left picture, in clock-wise order: picture of the entire 50 m decay region; detail of the target pile region; detail of the horn; detail of the target.

by running `BooNEG4Beam` with the `VRML2FILE` graphics system, and then creating snapshots of the graphics scene from the `vrmlview` VRML viewer. The geometry is identical to the G3 one.

3.2 Event generator

The event generator in `BooNEG4Beam` is very simple: all that is needed is to construct one primary proton per event with 8 GeV kinetic energy, directed towards the Be target. To account for the fact that the beam optics is not perfect, some smearing in the initial transverse position (x, y) and angular divergence (θ_x, θ_y) of the beam can be introduced. The position and angular smearing are described by gaussian distributions. More specifically, the initial position and momentum of the generated primary proton are:

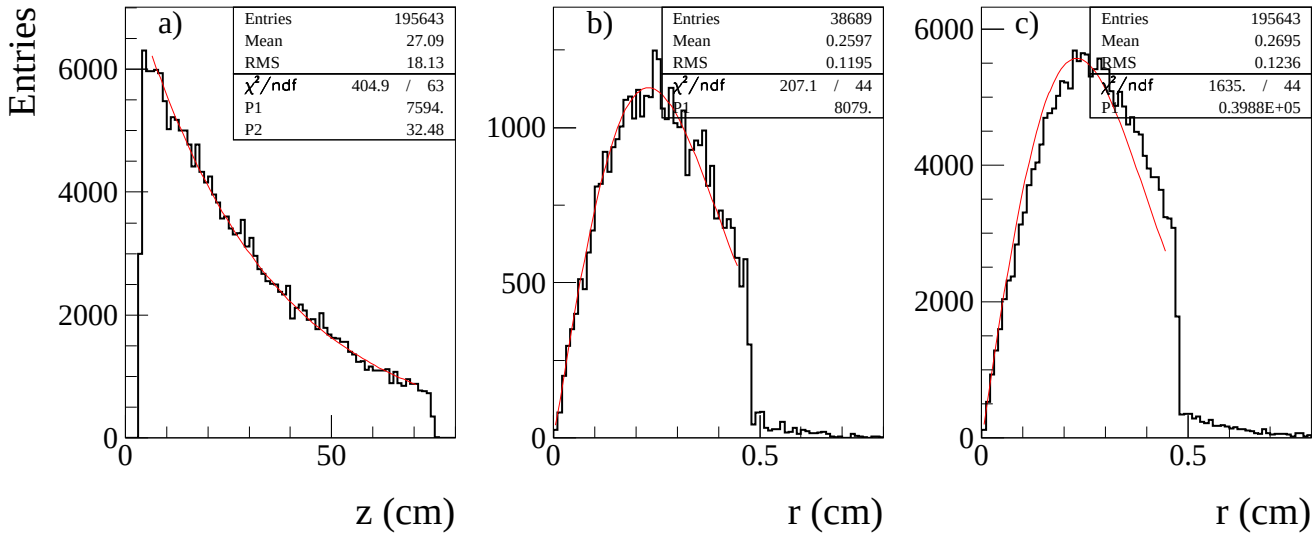

Figure 3: Validation of G4 primary beam description. a) longitudinal position z of the primary proton interaction point in the Be target; b) radial position r of the primary proton interaction in the Be target for $z < 10$ cm interactions; c) b) radial position of the primary proton interaction in the Be target for interactions occurring at all z-values. The black histograms refer to the G4 output, the solid red lines to the simple analytical expectations discussed in the text.

$$\begin{cases} x = \sigma_x \texttt{ran1} \\ y = \sigma_y \texttt{ran2} \\ z = -200 \text{ cm} \\ p_x = E_p \sigma_{\theta_x} \texttt{ran3} \\ p_y = E_p \sigma_{\theta_y} \texttt{ran4} \\ p_z = \sqrt{E_p^2 - m_p^2 - p_x^2 - p_y^2} \end{cases} \quad (1)$$

where `ran1`, `ran2`, `ran3`, `ran4` are four random numbers drawn from a gaussian distribution centered at zero and with an RMS of one, $E_p = K_p + m_p$, where K_p=8 GeV and m_p is the proton mass, and σ_x, σ_y, σ_{θ_x}, σ_{θ_y} are four parameters that can be set by the user in the `jobOptions.in` file. The default values are: $\sigma_x = \sigma_y = 0.15$ cm, $\sigma_{\theta_x} = \sigma_{\theta_y} = 0.05°$. The origin of the global coordinates system is the intersection between the target axis and the plane defining the upstream face of the horn. The choice $z = 200$ cm was made somewhat arbitrarily, and should be modified according to the beam parameters (for example, choosing $z = 0$ instead of $z = -200$ cm would slightly increase the neutrino flux normalization in MiniBooNE); the choice of p_z fixes the kinetic energy of all primary protons to be exactly 8 GeV, and could be modified as well according to beam measurements. Also, there are experimental indications that the nominal values for σ_x, σ_y, σ_{θ_x}, σ_{θ_y} are not accurate, and should be modified in the near future.

The black histograms in Fig.3 show the longitudinal (z) and transverse ($r \equiv \sqrt{x^2 + y^2}$) position for the first inelastic collision of primary protons in Beryllium. The z position distribution shown in Fig.3a) is discussed in Section 4; on the other hand, the r distributions shown in Figs.3b) and

c) for $z < 10$ cm and for all z values, respectively, can be in large part understood by the primary beam optics just described.

Along the x direction, at the upstream face of the target the x distribution is expected to be a gaussian, centered at zero and with width:

$$\sigma_{x,\theta_x} \simeq \sqrt{\sigma_x^2 + (l \cdot \sigma_{\theta_x})^2}$$

where $l \equiv 200$ cm, and σ_x and σ_{θ_x} have been defined above. A similar gaussian width is expected along the y direction. Therefore, $r = \sqrt{x^2 + y^2}$ is expected to be roughly distributed according to:

$$p(r) = \texttt{P1} \cdot r \cdot \exp\left[-r^2/(2\sigma_{x,\theta_x}^2)\right] \quad (2)$$

The red lines in Figs.3b) and c) show the above functional form, fitting only for the normalization parameter `P1`. The fit is done on the range $0 < r < 0.45$ cm, since the Be target core extends up to $r < 0.48$ cm [1]. The G4 r distribution for primary protons follow reasonably well the expected curve for $z < 10$ cm (Fig.3b) but it is slightly broader in the all-z case (Fig.3c). This is due to two reasons:

1. because the interaction lenght is nonzero, the average inelastic interaction point is located at $z > 0$, not $z = 0$: one should really use $l > 200$ cm in the above formula. This effect is minimized by selecting $z < 10$ cm events only;

2. in general, before interacting inelastically, the proton may have undergone a number of other physics processes, such as elastic collisions, ionisation, and multiple Coulomb scattering, which will tend to broaden the r distribution. The impact of all these physics processes is discussed in the Section 4. This effect is minimized by selecting $z < 10$ cm events only.

[1] There is some Be material at $r > 0.48$ cm: that is why the black histogram in Figs.3b) and c) shows a tail.

4 Code validation 2: individual physics processes

4.1 The MiniBooNE physics list

As discussed in Section 2, the classes `BooNEPhysicsList`, `BooNEHadronPhysics`, `ExN04EMPhysics`, `ExN04GeneralPhysics`, `ExN04IonPhysics`, and `ExN04MuonPhysics` register all physics processes to be used in the G4 simulation. Physics processes are chosen by instantiating a certain physics model describing that process; different particle types have in general a different list of physics processes registered and/or different models describing a given process. In addition, for a given particle type, different models can be selected according to the kinetic energy of the particle and the target material that the particle is traversing.

In this section, we validate some of the physics processes of greatest relevance to MiniBooNE by adopting the following simple philosophy: we turn off all of the physics processes in `BooNEG4Beam`, except the one we are interested in, and we analyse the outcomes of the simulation. We repeat this method for a number of conditions: different processes, particle types, momenta, materials.

In `BooNEG4Beam`, only one physics model does not belong to the fairly extensive list of choices available among the built-in G4 models (for more details on the built-in G4 physics models, the reader should consult the "Physics Reference Manual" available at [4]): this is a custom-defined model describing inelastic collisions of protons with a kinetic energy 7.5 GeV $< K_p <$ 8.5 GeV in Beryllium only. We start this Section by discussing this particular model, then we discuss the other physics processes affecting the MiniBooNE neutrino flux.

4.2 Particle production in Beryllium

For 7.5 GeV $< K_p <$ 8.5 GeV protons in Beryllium, the final state of all inelastic interactions is described by the `BooNEpBeInteraction` class. This is the physics process whose uncertainties affect the most the neutrino flux in MiniBooNE, and the one about which we seek to gather as much information as possible from past particle production experiments, BNL E910, and HARP.

What `BooNEpBeInteraction` does can be described by the following steps:

1. given one of the physics models supported by `BooNEpBeInteraction`, the average multiplicity per inelastic collision for various secondary particles is computed. There are currently six types of particles produced by each of the four models of proton-Beryllium inelastic collisions implemented: secondary protons, π^+, π^-, K^+, K^-, K^0_L; therefore, six multiplicities are computed. This is done once for the entire G4 simulation. The average multiplicity per inelastic collision is computed by dividing the inclusive production cross-section for each given secondary particle type by the total proton-Beryllium inelastic cross-section, σ_{inel}. The inclusive production cross-sections are given in the form of tables of double-differential cross-sections, as a function of longitudinal (p_z) and transverse (p_t) momentum for the secondary particle, with respect to the initial projectile direction. The numbers in the cross-section tables are given in units of $mb/(GeV/c)^2$. The numerator in the above ratio defining the average multiplicity per inelastic interaction is given by summing the double-differential cross-section over all (p_z, p_t) bins;

G4 Model	σ_{inel} (mb)	Physics model used for secondary particle production					
		p	π^+	π^-	K^+	K^-	K^0_L
`GFLUKA`	199.7	G	G	G	G	G	G
`MARS`	204.5	M	M	M	M	M	M/G
`ZGS`	any	M	Cho S-W fit	Cho S-W fit	M	M	M/G
`SWPar`	any	M	any S-W fit	any S-W fit	M	M	M/G

Table 1: Inleastic p-Be cross-section σ_{inel} and physics models used in the four G4 models for describing particle production in p-Be interactions. The abbreviation "G" refers to the GFLUKA model, "M" to the MARS model, "S-W" to the Sanford-Wang parametrization described in the text.

2. when `BooNEpBerInteraction` is called by the G4 process manager, the number and composition of final state particles is selected by drawing six multiplicity numbers, one for each of the secondary particle types, from Poisson distributions with the average multiplicities calculated. The corresponding particles are then created as daughter particles of the projectile particle;

3. for each of the final state particles created, their 3-momentum is assigned according to the double-differential cross-section tables. This is done by applying a simple accept/reject method to the 2-dimensional (p_z, p_t) probability distribution function, obtained from a linear interpolation of the disctretized $\Delta^2\sigma/\Delta p_z \Delta p_t$ cross-section table. The cross-section table contains 50×100 $p_z \times p_t$ bins over the ranges $(0 < p_z < 10$ GeV/c$, 0 < p_t < 1$ GeV$)$;

4. the momentum vector of the secondary particle is rotated according to the initial projectile direction;

5. the original incidient particle as well as the struck Be nucleus are deleted from the particle stack;

6. if requested, ntuple 2000 with the secondary particles information is filled. This is optional, and present for debugging purposes only. This ntuple being filled at the process level of the simulation, while the default ntuple 1000 is being filled at the event level (see Fig.1 to see the relation between event and processes).

The `BooNEG4Beam` user can currently choose among four different types of physics models: `GFLUKA`, `MARS`, `ZGS`, `SWPar`. The assumptions for these models are explained below, and are summarized in Tab.1.

`GFLUKA` : p, $\pi^{\pm}$, $K^{\pm}$, K^0_L production is described according to the cross-section tables contained in the file `GFLUKAData.hh` in the `physics/` subdirectory. These six cross-section tables were all extracted from an *ad hoc* GEANT3.21 simulation of 25 million 8 GeV protons traversing a thin block of Be material, choosing the FLUKA physics option in GEANT3.21. The GFLUKA inelastic cross-section in p-Be interactions of 199.7 mb is obtained by using the `PLMAT` command in GEANT3.21;

`MARS` : p, $\pi^{\pm}$, $K^{\pm}$ production is described according to the cross-section tables contained in the file `MARSData.hh` in the `physics/` subdirectory. These five cross-section tables were all extracted

from an *ad hoc* MARS14 simulation of 10 million 8 GeV protons in Beryllium, as well as the MARS p-Be inelastic cross-section (204.5 mb). A different approach was used for K^0_L, given the fact that MARS does not store K^0_L particles. In this case, the K^0_L yield in any (p_z, p_t) bin is constructed from the MARS K^+ yield, times the GFLUKA K^0_L/K^+ yield ratio:

$$\frac{d^2N_{K_L,MARS}}{dp_z dp_t} \equiv \frac{d^2N_{K^+,MARS}}{dp_z dp_t} \cdot \left(\frac{d^2N_{K_L,GFLUKA}}{dp_z dp_t} \Big/ \frac{d^2N_{K^+,GFLUKA}}{dp_z dp_t}\right)$$

This is the meaning of the abbreviation "M/G" under K^0_L for the `MARS` G4 model in Tab.1;

`ZGS` : $\pi^\pm$ production is described according to the Sanford-Wang parametrization of $\pi^\pm$ production data from Argonne's ZGS data, described in [8]. The Sanford-Wang parametrization for the $\pi^\pm$ inclusive double-differential cross-section is defined by sixteen parameters, $c^\pm_1, \ldots, c^\pm_8$, eight for π^+ production, eight for π^- production:

$$\frac{d^2\sigma(p + Be \to \pi^\pm + X)}{dpd\Omega} = c^\pm_1 p^{c^\pm_2} \left(1 - \frac{p}{p_{beam} - 1}\right) \exp\left[-c^\pm_3 \frac{p^{c^\pm_4}}{p^{c^\pm_5}_{beam}} - c^\pm_6 \vartheta (p - c^\pm_7 p_{beam} \cos^{c^\pm_8} \vartheta)\right] \tag{3}$$

These sixteen parameters are chosen as in [8], and the cross-section tables are filled according to this Sanford-Wang parametrization. Instead, p, $K^\pm$, K^0_L production is described in the same way as for the `MARS` model. The total inelastic cross-section σ_{inel} can be chosen by the user via the user interface command `/boone/physics/ZGSpBeInelasticXSec`, defined in `BooNEpBeInteractionMessenger`; its default value is 204.5 mb;

`SWPar` : $\pi^\pm$ production is described according to two custom-defined Sanford-Wang parametrizations, where the user sets the value of the sixteen $\pi^\pm$ production parameters via the commands `/boone/physics/SWPiPlusPar` and `/boone/physics/SWPiMinusPar`. The cross-section tables for $\pi^\pm$ production are filled accordingly. The default values for the π^+ parameters are the central values for the JAM combined fit of existing π^+ production data in p-Be interactions, as described in [9] by Jocelyn Monroe. The default values for the π^- parameters are the values from the fit in [8] by Cho *et al.*. p, $K^\pm$, K^0_L production is described in the same way as for the `MARS` model. The total inelastic cross-section for this model can be chosen by the user via the user interface command `/boone/physics/SWParpBeInelasticXSec`, its default value is 204.5 mb. The ν_e,$\bar{\nu}_e$,ν_μ,$\bar{\nu}_\mu$ fluxes at the MiniBooNE detector obtained from this model, with the default values just described, were used for the WIN03 Monte Carlo production (`2003-08-15` MC files). In this note, we refer to this model as to the `JAM` model.

We note that there are no requirements on conservation of quantities such as electric charge, baryon number, momentum, or energy, in inelastic interactions as described by `BooNEpBeInteraction`; the reason is threefold:

1. not all secondary particles are being produced, only the ones relevant to the neutrino fluxes;
2. as can be seen in Tab.1, different (and not necessarily consistent) models are used for different secondaries within a physics model;
3. the algorithm in `BooNEpBeInteraction` described above for creating secondaries is meant to give reasonable results only in a statistical sense, not on an event-by-event basis. Of course, this should not have any effect on the MiniBooNE neutrino fluxes, which require the

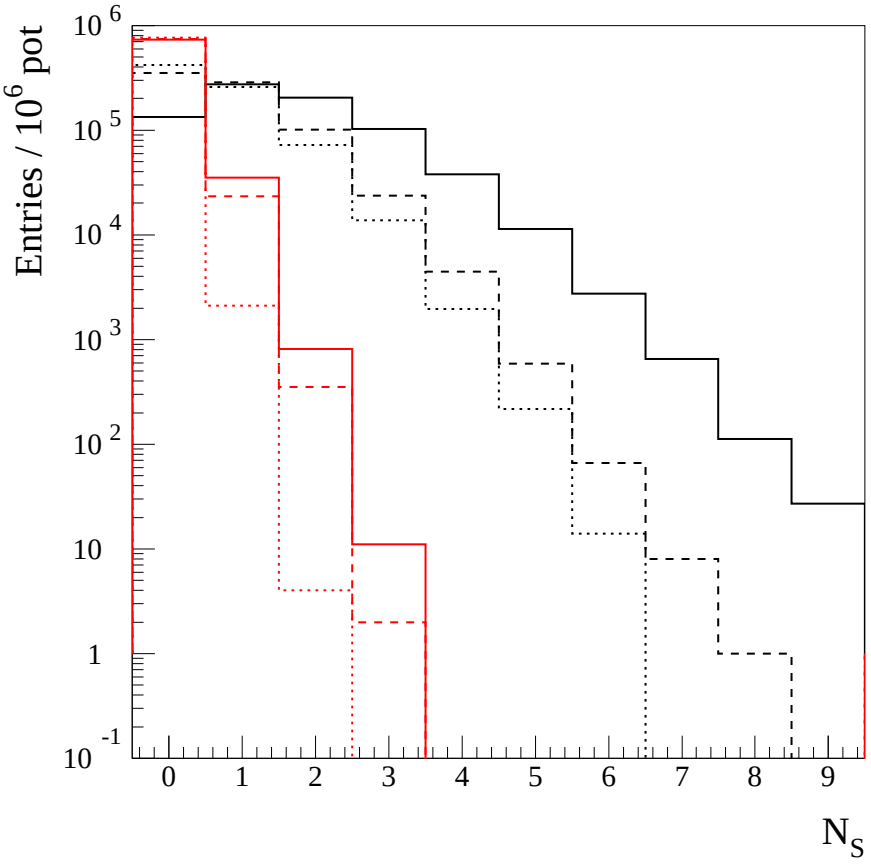

Figure 4: Multiplicity distributions per inelastic collision, N_S, for secondary particles produced in inelastic collisions of primary protons in a Be target, from the G4 simulation. Black solid line: secondary protons; black dashed line: π^+; black dotted line: π^-; red solid line: K^+; red dashed line: $K^)_L$; red dotted line: K^-.

simulation of at least 10^6 protons on target. On the contrary, the absence of any requirements on particle correlations (in other words, the inclusive approach) makes it easier to interface additional experimental data to `BooNEG4Beam`, and is preferred.

A number of cross-checks have been made to make sure that the `BooNEpBeInteraction` class correctly describes particle production in p-Be inelastic interactions. We start by looking at the multiplicity per inelastic collision, N_S, obtained with the `JAM` model G4 simulation, for the various secondary particle types $S = p, \pi^{\pm}, \ldots$. Fig.4 shows the N_S distribution for p, $\pi^{\pm}$, $K^{\pm}$, K^0_L production. The number of entries in the histogram correspond to 10^6 protons on the MiniBooNE target simulated in `BooNEG4Beam`, as stored in ntuple 2000.

In Tab.2, the average multiplicities from the distributions in Fig.4 are given in the μ_S^{obs} column. The μ_S column in Tab.2 is the expected multiplicity per inelastic colision given the inclusive cross-

Secondary particle type S	Average Multiplicity per inelastic collision		
	μ_S^{obs}	μ_S	μ_S^{corr}
p	$1.59 \cdot 10^{0}$	$1.50 \cdot 10^{0}$	$1.59 \cdot 10^{0}$
π^+	$7.55 \cdot 10^{-1}$	$7.10 \cdot 10^{-1}$	$7.54 \cdot 10^{-1}$
π^-	$5.92 \cdot 10^{-1}$	$5.58 \cdot 10^{-1}$	$5.93 \cdot 10^{-2}$
K^+	$4.81 \cdot 10^{-2}$	$4.51 \cdot 10^{-2}$	$4.79 \cdot 10^{-2}$
K_L	$3.12 \cdot 10^{-2}$	$2.95 \cdot 10^{-2}$	$3.14 \cdot 10^{-2}$
K^-	$2.76 \cdot 10^{-3}$	$2.64 \cdot 10^{-3}$	$2.80 \cdot 10^{-3}$

Table 2: Average multiplicity per inelastic collision for secondary particles produced in inelastic collisions of primary protons in a Be target. The μ_S^{obs} column refers to the means of the distributions in Fig.4. The μ_S column is the multiplicity expected, given the cross-section tables used by G4 in the simulation. In the μ_S^{corr} column, inelastic interactions with no protons, charged pions, or kaons are neglected in calculating the expected average multiplicity. The μ_S^{obs} numbers should be compared to the μ_S^{corr} ones (see text for details).

section tables and the total inelastic cross-section σ_{inel}:

$$\mu_S = (\sum_{ipz=1}^{100}\sum_{ipt=1}^{50}\frac{\Delta^2\sigma(p+Be\rightarrow S+X)}{\Delta p_z \Delta p_t})/\sigma_{inel} \tag{4}$$

for a secondary type S. Now, the G4 output multiplicity is expected to be slightly higher than the one predicted by a Poisson distribution with mean μ_S, since no information is recorded by G4 if zero secondary particles are produced in the interaction [2]. More precisely, the expected average multiplicities from the G4 output are expected to be:

$$\mu_S^{corr} = \frac{\sum_{N_S=0}^{\infty} N_S \cdot P^{corr}(N_S,\mu_S)}{\sum_{N_S=0}^{\infty} P^{corr}(N_S,\mu_S)} \tag{5}$$

where:

$$\begin{cases} P^{corr}(N_S>0,\mu_S) = P(N_S>0,\mu_S) \\ P^{corr}(N_S=0,\mu_S) = P(N_S=0,\mu_S)\cdot\epsilon_S \end{cases} \tag{6}$$

where $P(N_S,\mu_S)$ is the Poisson distribution with mean μ_S, and the correction factor ϵ_S for the secondary particle type S is given by:

$$\epsilon_S = \prod_{S'\neq S} P(N_{S'}>0,\mu_{S'}) \tag{7}$$

From Tab.2, the observed average multiplicities per inelastic collision, μ_S^{obs}, are consistent with the expected multiplicities μ_S^{corr}.

Having verified that the particle multiplicitites are as expected, we now examine the final state kinematics of the particles. Fig.5 shows the 2-dimensional (p_z, p_t) distributions for the momenta of the six secondary particle types produced, p, $\pi^{\pm}$, $K^{\pm}$, K_L^0. The number of entries in the histograms

[2]Note that this situation can happen in the simulation, since the G4 simulation is only correct in a statistical sense and not event-by-event, as previously described.

correspond to simulating 10^6 protons on the MiniBooNE target, using the `JAM` production model.

In the case of $\pi^{\pm}$ production, we can directly compare the distributions in Fig.5 with the known Sanford-Wang $\pi^{\pm}$ parametrizations used in the `JAM` model. The ratio of the two distributions, simulated in GEANT4 versus theoretical, is shown in Fig.6 for both π^+'s and π^-'s.

The distributions are normalized in order to represent the same number of inelastic interactions. We observe no systematic biases with respect to expectations in the `BooNEpBeInteraction` secondary momentum distributions.

Finally, we should consider the pathlength distribution of a primary proton in Beryllium before it interacts inelastically. Different distributions can give:

1. slightly different overall neutrino fluxes. This effect is minimized by the fact that the MiniBooNE target is thick, $\sim 1.7\lambda_{inel}$, and the vast majority of protons interact inelastically within the target regardless of the exact value of λ_{inel};
2. slightly different neutrino energy distributions, as the momentum acceptance of the horn slightly changes depending on the average entry position of mesons in the magnetic field region.

In principle, the inelastic interaction length λ_{inel} should be fixed by the inelastic cross-section σ_{inel} that we defined in all `BooNEpBeInteraction` physics models, via:

$$\lambda_{inel} = \frac{A}{\rho N_{Av} \sigma_{inel}} \tag{8}$$

where $A = 9.01\ g/mol$ is the Beryllium atomic weight, $\rho = 1.848\ g/cm^3$ is the Beryllium density, $N_{Av} = 6.022 \cdot 10^{23}\ mol^{-1}$ is Avogadro's number. In practice, the inelastic cross-section defined by the user only affects the secondary particles *multiplicity* per inelastic collision once an inelastic interaction occurs, not *where* the inelastic interaction occurs in the first place. The inelastic cross-section used to determine the interaction vertex is, in `BooNEG4Beam`, given by one of the G4 built-in models, the "Low Energy Parametrization Driven Model", based on the GEANT3.21 GHEISHA package (see the "Physics Reference Manual" at [4] or browse the code at `$G4INSTALL/source/processes/hadronic/cross_` for further details). Fig.3a) in the Section 3 shows the distribution for the inelastic interaction longitudinal position z. The red curve is a fit to the G4 histogram based on the funcptional form:

$$f(z) = \texttt{P1}(1 - \exp(-z(cm)/\texttt{P2})) \tag{9}$$

The fit, performed along the MiniBooNE Be target length, gives for the G4 built-in inelastic interaction length:

$$\lambda_{inel} \equiv \texttt{P2} \simeq 32.5 \text{ cm}$$

corresponding to (see Eq.8) $\sigma_{inel} \simeq 249$ mb, a little higher compared to the currently preferred values ($\simeq 200 - 210$ mb), but probably not as different as to produce a large bias in the MiniBooNE neutrino flux, given the thickness of the MiniBooNE target.

In principle, it is possible in GEANT4 to tailor the reaction cross-section data store according to the users' needs, and not only the model describing the final state for that reaction. This is currently not implemented in `BooNEG4Beam`.

4.3 Other inelastic processes

Secondary interactions of pions and protons play a non-negligible role in determining the MiniBooNE neutrino flux. These particles, once they have been created in a primary inelastic interaction, can still traverse significant amounts of target and horn material (relative to the inelastic interaction length), and in turn interact inelastically. Therefore, we study here inelastic interactions of secondary pions and protons of various momenta in Beryllium and Aluminum. These studies are made by defining pions and protons of various momenta as the G4 generated primaries, and studying their inelastic interactions in traversing simple geometries: 2 meters long blocks of Be and Al materials. In particular, we are interested in:

1. the interaction length used by GEANT4 for inelastic interactions of pions and protons in Beryllium and Aluminum, as a function of the projectile momentum;

2. the multiplicity and momentum distribution of the π^+'s in the final state of such processes, since this information affects the MiniBooNE ν_μ flux.

These inelastic processes, with the exception of $K_p > 7.5$ GeV protons in Beryllium discussed above, are described by the `G4LEPionPlusInelastic` and `G4LEProtonInelastic` classes. These classes are part of the 'Low Energy Parametrization Driven Model", based on the GEANT3.21 GHEISHA package (see the "Physics Reference Manual" at [4] for further details, or browse the source code at `$G4INSTALL/source/processes/hadronic/models/low_energy/`). The π^+ charge exchange reaction is included in the inelastic reaction.

Fig.7 shows various distributions obtained from such inelastic processes: the interaction position projected along the direction of the projectile, the π^+ multiplicity, the π^+ momentum, the π^+ angle with respect to the projectile direction.

Tab.3 summarizes the information on the inelastic interaction length and π^+'s in the final state contained in Fig.7. The inelastic interaction lengths given in Tab.3 are obtained via an exponential fit to the z distributions, of the form given in Eq.9. The inelastic interaction lengths for π^+'s and protons are similar, of the order of 40 cm. The Particle Data Group [10] quotes the values 75.2 and 106.4 g/cm^2 for the inelastic interaction lengths per unit density in Beryllium and Aluminum, respectively, corresponding to 40.7 and 39.4 cm for Be and Al, respectively. The G4 inelastic cross-sections show a mild energy dependence: over the range 1-5 GeV/c, the interaction length is smallest for low-energy pions and high-energy protons.

Pions in the final state tend to be more numerous for higher energy projectiles, for π^+ projectiles than for p projectiles, and show little dependence on the target material. Note that the predictions for the inelastic model used for secondary proton interactions are not necessarily consistent with the predictions from the model used in primary proton inelastic interactions. The `JAM` model used for the latter process gives a pion multiplicity of 0.90 at 8.9 GeV/c protons in Beryllium [3], while the G4 built-in model `G4LEPionPlusInelastic` gives the similar value of 0.88 at the much smaller proton momentum of 5 GeV/c (see Tab.3). The average π^+ momentum tends to be much smaller than the projectile momentum, and π^+ emission angles ave large.

[3]The value 0.71 given for this multiplicity in Tab.2 refers to $p_t < 1$ GeV/c pions; pions with higher p_T values do not contribute to the MiniBooNE neutrino flux, as shown in Section 6.

Projectile	Target material	Proj. momentum (GeV/c)	λ_{inel} (cm)	$\langle N_{\pi+}\rangle$	$\langle p_{\pi+}\rangle$ (GeV/c)	$\langle \theta_{\pi+}\rangle$ (π)
π^+	Be	1	38.8	0.42	0.30	0.32
π^+	Be	3	44.7	0.68	0.56	0.21
π^+	Be	5	53.1	1.06	0.74	0.21
π^+	Al	1	37.8	0.39	0.22	0.35
π^+	Al	3	41.4	0.68	0.47	0.21
π^+	Al	5	48.7	1.19	0.61	0.25
p	Be	1	47.6	0.43	0.10	0.27
p	Be	3	38.3	0.57	0.41	0.23
p	Be	5	39.2	0.88	0.54	0.24
p	Al	1	46.2	0.08	0.09	0.26
p	Al	3	38.1	0.55	0.35	0.24
p	Al	5	37.1	0.96	0.45	0.27

Table 3: Inelastic interaction length λ_{inel}, average π^+ multiplicity $\langle N_{\pi+}\rangle$, average momentum $\langle p_{\pi+}\rangle$ and angle $\langle \theta_{\pi+}\rangle$ of π^+'s in the final state, in inelastic collisions of π^+'s and protons of 1, 3, 5 GeV/c momentum in Beryllium and Aluminum. This table summarizes the information contained in Fig.7.

4.4 Elastic processes

Apart from scattering inelastically, pions and protons also interact elastically in the Be and Al materials. This process is simulated by the `G4LElastic` class. In this case, no particle absorption, particle production, or charge exchange occurs: the only effect is an angular deflection of the projectile with respect to its original direction. Therefore, we wish to study:

1. what is the distance travelled before an elastic interaction occurs in Beryllium and Aluminum, for pions and protons of various momenta? This is shown in the top plots of Fig.8;
2. what is the deflection angle with respect to the projectile direction when such elastic interactions occur? This is shown in the bottom plots of Fig.8;

Given the distributions in Fig.8, we can extract the elastic interaction length λ_{el} (via an exponential fit to the z distributions, Eq.9) and the average deflection angle in elastic interactions. The results for the various projectiles, target materials, projectile momenta considered are shown in Tab.4.

The elastic interaction is smaller in Aluminum than in Beryllium, and very similar for protons or pions; the elastic interaction length is in the range 110-165 cm for the Be target, 65-95 cm for the Be target, significantly larger than the corresponding inelastic interaction lengths. Using the formula:

$$\frac{1}{\lambda_T} = \frac{1}{\lambda_{el}} + \frac{1}{\lambda_{inel}} \tag{10}$$

where λ_T is the total nuclear collision length, and the PDG values for λ_T and λ_{inel} [10], we get 117.0 and 77.7 cm for Be and Al, respectively; again, there is good agreement between G4 and the PDG values. The elastic cross-section tend to be higher at low momenta.

Projectile	Target material	Proj. momentum (GeV/c)	λ_{el} (cm)	$\langle\theta\rangle$ (π)
π^+	Be	1	111.6	0.053
π^+	Be	3	153.0	0.018
π^+	Be	5	164.6	0.011
π^+	Al	1	65.1	0.037
π^+	Al	3	86.6	0.013
π^+	Al	5	96.3	0.007
p	Be	1	121.1	0.053
p	Be	3	111.8	0.018
p	Be	5	143.2	0.011
p	Al	1	68.5	0.037
p	Al	3	63.0	0.012
p	Al	5	77.9	0.007

Table 4: Elastic interaction length λ_{el} and average projectile deflection angle $\langle\theta\rangle$ with respect to the incident projectile direction in elastic interactions of π^+'s and protons of 1, 3, 5 GeV/c momentum in Beryllium and Aluminum. This table summarizes the information contained in Fig.8.

The mean deflection angles are much smaller in elastic collisions than in the previosuly discussed inelastic collisions. The angles tend to be larger, on average, for low-energy projectiles in Beryllium, and again are very similar for protons and pions. Typical deflection angles in one elastic collision are 20-160 mrad.

4.5 Ionisation by charged hadrons

Having discussed the "microscopic" elastic and inelastic processes, we now turn to "macroscopic" effects of particle interactions in matter. We consider first energy loss processes by charged hadrons. The G4 class `G4hIonisation` simulates both the continuous energy loss due to ionisation and atomic excitation via the Bethe-Bloch formula, as well as the "discrete" part of the ionisation via δ-ray emission. We wish to study:

1. what is the energy loss of a pion or proton in traversing a certain material thickness?
2. what is the typical deflection angle due to ionisation after a certain material thickness?

We have simulated the ionisation characteristics for 1, 3, and 5 GeV/c protons and π^+'s in traversing 10 cm thick blocks of Beryllium and Aluminum. We define Δ as the projectile energy loss across the 10 cm of material:

$$\Delta \equiv -\int_0^{10\ \mathrm{cm}} \frac{dE}{dz} dz \tag{11}$$

In Fig.9, top plots, we show the Δ/z distributions for various cases. The curves have the characteristic aspect of Landau distributions, with a long tail at high energy losses per unit distance. The bottom plots in Fig.9 show the deflection angles after traversing 10 cm of material.

The information contained in Fig.9 is summarized in Tab.5. The average energy losses per unit distance are higher in Aluminum than in Beryllium, as expected. The PDG [10] gives, for both

Projectile	Target material	Proj. momentum (GeV/c)	$\langle\Delta/z\rangle$ (MeV/cm)	$\langle\theta\rangle$ at z=10 cm (mrad)
π^+	Be	1	3.03	1.73
π^+	Be	3	3.17	0.70
π^+	Be	5	3.18	0.44
π^+	Al	1	4.50	2.08
π^+	Al	3	4.74	0.89
π^+	Al	5	4.81	0.56
p	Be	1	4.48	0.79
p	Be	3	2.99	0.48
p	Be	5	2.98	0.33
p	Al	1	6.52	0.78
p	Al	3	4.35	0.57
p	Al	5	4.40	0.41

Table 5: Summary on the G4 energy loss results shown in Fig.9. The average energy loss per unit distance traversed, Δ/z, and the average deflection angle due to ionisation after 10 cm of material, $\langle\theta\rangle$, are given as a function of projectile type, momentum, and target material.

Beryllium and Aluminum, the following values for the minimum energy loss per material density:

$$-\frac{1}{\rho}(\frac{dE}{dz})_{min} \simeq 1.6\ MeV\ g^{-1}\ cm^2$$

yielding $\simeq 3.0$ and $\simeq 4.3\ MeV/cm$ for the minimum energy losses per unit distance in Beryllium and Aluminum, respectively. The PDG values are consistent with the G4 values in Tab.5. Note that at low momenta, 1 GeV/c, the increase in energy loss is much larger for protons than for pions, as expected.

Tab.5 also shows the mean deflection angle after traversing 10 cm of material. These angles are very small, of the order of 1 mrad, and negligible with respect to the deflection angles due to multiple Coulomb scattering, which we treat next.

4.6 Multiple Coulomb scattering

The cumulative effect of the many small electromagnetic scatters that a charged particle undergoes in matter is described by the `G4MultipleScattering` class. This model does not use the Molière formalism, but is based on the more complete Lewis theory [4]. As for the energy loss, we have simulated the effect of this process for pions and protons traversing 10 cm thick Be and Al blocks. We wish to know:

1. what is the scattering angle with respect to the original projectile direction, due to multiple Coulomb scattering (MCS)?

The scattering angle distributions for 1, 3, 5 GeV/c pions and protons in Beryllium and Aluminum are shown in Fig.10.

Projectile	Target material	Proj. momentum (GeV/c)	$\langle\theta\rangle_{G4}$ at z=10 cm (mrad)	$\langle\theta\rangle_H$ at z=10 cm (mrad)
π^+	Be	1	9.4	8.7
π^+	Be	3	3.2	2.9
π^+	Be	5	1.9	1.7
π^+	Al	1	19.0	18.3
π^+	Al	3	6.3	6.1
π^+	Al	5	3.8	3.6
p	Be	1	13.0	11.9
p	Be	3	3.3	3.0
p	Be	5	1.9	1.8
p	Al	1	26.4	24.9
p	Al	3	7.0	6.3
p	Al	5	4.1	3.7

Table 6: Average projectile deflection angles, after traversing 10 cm of material, due to multiple Coulomb scattering, as predicted by GEANT4 ($\langle\theta\rangle_{G4}$) and by the Highland formula given by the PDG ($\langle\theta\rangle_H$), for different projectile types, momenta, and target materials.

Tab.6 gives the average G4 deflection angles due to multiple Coulomb scattering, $\langle\theta\rangle_{G4}$, as obtained from Fig.10. GEANT4 predicts larger scattering angles for low-momentum projectiles, larger scattering angles in Aluminum than in Beryllium, and similar scattering angles for pions and protons of same momentum, with the exception of low-momentum particles where the scattering angle for protons is larger than for pions. Typical scattering angles over 10 cm of material are between 2 and 26 mrad.

These results can be confronted with the Highland formula given by the PDG [10], describing the average MCS deflection angle $\langle\theta\rangle$:

$$\langle\theta\rangle_H = \sqrt{\frac{\pi}{2}}\sigma_\theta \tag{12}$$

where:

$$\sigma_\theta = \frac{13.6 \text{ MeV}}{\beta cp}\sqrt{z/X_0}[1 + 0.038\ln(z/X_0)] \tag{13}$$

In Eq.13, βc is the projectile velocity, p its momentum, $z \simeq 10$ cm is the material traversed, X_0 is the material radiation length, which is 35.28 cm for Be and 8.9 cm for Al [10]. In Tab.6, we report also the average deflection angle due to multiple Coulomb scattering as predicted by the Highland formula: the G4 and Highland average deflection angles are very close to each other.

4.7 Particle trajectories in horn magnetic field

The horn magnetic field provides a large (×7) increase in flux, and is therefore necessary to accurately check the motion of charged particles in the field. In GEANT4, as in GEANT3, the user has the capability to "attach" magnetic field attributes to a specific logical volume, in this case the horn logical volume "HRN1". In G4, this is done in the `BooNEGeometryConstruction`

class. The magnetic field map is specified in the `BooNELocalField` class. The messenger class `BooNELocalFieldMessenger` allowes the user to specify the horn current in the `jobOptions.in` file.

Fig.11 shows two different views of the same three π^+ tracks, produced at ($x = 3$ cm, $y = 0$, $z = 40$ cm), ($\theta_x \equiv \arctan(p_x/p_z) = 7°$, $\theta_y \equiv \arctan(p_y/p_z) = 0$), and kinetic energies of 0.15, 2.0, 5.0 GeV. The angle of 7° is chosen because it is a characteristic angle for pion production giving neutrinos in MiniBooNE (see Section 6).

The π^+ trajectories in Fig.11 show all the qualitative features to be expected. Out of the three tracks, only the 2.0 GeV one reaches the end of the collimator folowing the horn without interacting in the surrounding material, while the 5.0 GeV is underfocused and the 0.15 GeV is overfocused. Moreover, the track deflection is apparent only in the region comprised between the horn inner and outer conductors, as it should be since this is the only region where a nonzero magnetic field is present.

A more quantitative test has also been performed. The case considered is that, for simplicity, of π^-'s produced parallel to the horn axis. The particle trajectory is checked by looking at which longitudinal position z_{max} the π^- crosses the inner surface of the horn outer conductor, because of magnetic defocusing. The horn outer conductor is located at a 30 cm transverse distance from the horn axis.

In this simple case, for particles with initial momentum directed along the horn axis, the motion occurs in a plane (x, z), where z is the projection on the horn axis direction, x is the distance from this axis. We then have to solve the following system of two coupled, second-order differential equations:

$$\begin{cases} \ddot{x}(t) = \frac{c_B}{x(t)}\dot{z}(t), & \dot{x}(0) = 0, \quad x(0) = x_0 \\ \\ \ddot{z}(t) = -\frac{c_B}{x(t)}\dot{x}(t), & \dot{z}(0) = v_0, \quad z(0) = z_0 \end{cases} \tag{14}$$

where, in SI units:

$$c_B = \frac{\mu_0 I}{2\pi} \cdot \frac{q}{m_\pi \gamma} \tag{15}$$

where $\mu_0 = 4\pi \cdot 10^{-7}$ is the permittivity of free space, I is the horn current, q is the (positive) electron charge, m_π the $\pi^\pm$ mass, γ is the relativistic γ factor for the pion.

This set of equations does not seem analytically solvable, and a numerical integration method by Runge-Kutta-Nystrom was used instead, in order to check the G4 results. The implementation used of this numerical method comes from the CERNLIB subroutine `DRKNYS`. The initial conditions used are ($x_0 = 3$ cm, $z_0 = 10$ cm), and initial velocity v_0 corresponding to π^- kinetic energies of 20, 140, 600 MeV. The trajectories as calculated by GEANT4 and by CERNLIB are shown in Fig.12.

Tab.7 shows z values for the 20, 140, 600 MeV π^- trajectories as they cross the outer conductor surface, at $x = 30$ cm, as calculated by both GEANT4 [4] and by CERNLIB. The results are consistent with each other in both the nonrelativistic and relativistic regimes.

[4]The volume between the inner and outer conductor was made of vacuum instead of air for this simulation.

K (MeV)	z_{max} (cm) from G4	z_{max} (cm) from CERNLIB
20	52.83	52.83
140	93.92	93.92
600	159.52	159.52

Table 7: Cross-check on G4 π^- defocusing due to the horn magnetic field, for π^- tracks of various kinetic energies K. The value of z_{max} indicates where the trajectories cross the $r = 30$ cm cylindrical surface of the horn outer conductor. The G4 results agree with those from a standalone calculation based on the CERNLIB subroutine `DRKNYS`.

Particle	Lifetime (ns)	Decay mode	Branching ratio (%)	G4 class
π^+	26.03	$\mu^+\nu_\mu$	100.0	`G4PhaseSpaceDecayChannel`
K^+	12.37	$\mu^+\nu_\mu$	63.5	`G4PhaseSpaceDecayChannel`
		$\pi^+\pi^0$	21.2	`G4PhaseSpaceDecayChannel`
		$\pi^+\pi^+\pi^-$	5.6	`G4PhaseSpaceDecayChannel`
		$\pi^0 e^+\nu_e$	4.8	`G4KL3DecayChannel`
		$\pi^0\mu^+\nu_\mu$	3.2	`G4KL3DecayChannel`
		$\pi^+\pi^0\pi^0$	1.7	`G4PhaseSpaceDecayChannel`
K^0_L	51.70	$\pi^0\pi^0\pi^0$	21.1	`G4PhaseSpaceDecayChannel`
		$\pi^- e^+\nu_e$	19.4	`G4KL3DecayChannel`
		$\pi^+ e^-\bar{\nu}_e$	19.4	`G4KL3DecayChannel`
		$\pi^-\mu^+\nu_\mu$	13.6	`G4KL3DecayChannel`
		$\pi^+\mu^-\bar{\nu}_\mu$	13.6	`G4KL3DecayChannel`
		$\pi^0\pi^+\pi^-$	12.6	`G4PhaseSpaceDecayChannel`
μ^+	2197.03	$e^+\nu_e\bar{\nu}_\mu$	100.0	`G4MuonDecayChannel`

Table 8: Particle lifetimes, and built-in decay modes and branching ratios, defined in GEANT4. The "G4 class" column list the classes responsible for the corresponding decay modes.

4.8 Particle decays

Neutrinos in the MiniBooNE detector are produced via the decays of charged pions, kaons, and muons. As far as particle decays are concerned, we wish to check in `BooNEG4Beam`:

1. what are the particles' lifetimes?
2. what are the decay branching ratios?
3. what is the final state kinematics of the neutrinos produced in the decays?

The user interface commands `/particle/property/dump` and `/particle/property/decay/dump` list the lifetimes and branching ratios used internally by GEANT4; those are reported in Tab.8 for π^+, K^+, K^0_L, and μ^+, together with the G4 classes responsible for simulating the decays.

Parent	Momentum (GeV/c)	$\gamma\beta c\tau$ (m)	λ_{G4} (m)	Neutrino	$\langle E_\nu/E_{parent}\rangle_{BooBeamNT}$	$\langle E_\nu/E_{parent}\rangle_{G4}$
π^+	1	55.9	55.9	ν_μ	0.213	0.213
	3	167.8	167.3	ν_μ	0.213	0.213
	5	279.6	278.2	ν_μ	0.213	0.213
K^+	1	7.5	7.5	ν_e	0.290	0.273
				ν_μ	0.467	0.464
	3	22.6	22.6	ν_e	0.291	0.266
				ν_μ	0.468	0.467
	5	37.6	37.4	ν_e	0.289	0.271
				ν_μ	0.468	0.466
K^0_L	1	31.2	31.2	ν_e	0.289	0.266
				ν_μ	0.293	0.237
	3	93.5	93.0	ν_e	0.291	0.266
				ν_μ	0.290	0.238
	5	155.8	155.2	ν_e	0.291	0.267
				ν_μ	0.290	0.238
μ^+	1	$6.23 \cdot 10^3$	$6.19 \cdot 10^3$	ν_e	0.401	0.326
				ν_μ	0.399	0.324
	3	$1.87 \cdot 10^4$	$1.88 \cdot 10^4$	ν_e	0.402	0.327
				ν_μ	0.399	0.325
	5	$3.12 \cdot 10^4$	$3.12 \cdot 10^4$	ν_e	0.402	0.325
				ν_μ	0.400	0.325

Table 9: Comparison on G4 decay processes from Fig.13 with, expectations from PDG numbers and from the `BooBeamNT` MiniBooNE redecay program. The G4 decay path lengths λ_{G4} agree well with the expected $\gamma\beta c\tau$ value, for all neutrino parent momenta. The G4 and `BooBeamNT` average values for the ratio between the neutrino energy E_ν and the total energy of the parent particle E_{parent} are consistent for π^+ decay only.

Lifetime values are consistent with the PDG values [10], and the most probable decay modes are present at the expected branching ratios. We note the absence of the $\pi^+ \to e^+\nu_e$ decay; even though the $\pi^+ \to e^+\nu_e$ decay is not one of the major sources of the intrinsic ν_e flux expected in MiniBooNE, its contribution might be non-negligible and should be added to the $\pi^\pm$ decay modes. The capability of adding extra decay modes to a particle is present in GEANT4.

We'd also like to check the final state kinematics of neutrinos arising from particle decays. In order to do this, we have simply constructed a large vacuum volume, let particles of given momenta decay, and recorded the information on the neutrinos momenta. The top plots in Fig.13 shows the z-distributions of π^+, K^+, K^0_L, and μ^+ decays, for 1, 3, 5 GeV/c parent momenta. The bottom plots show the ratios of the daughter neutrino energies divided by the total parent energy. In the bottom plots, the energy ratios for ν_e's and ν_μ's are shown separately.

The decay information from Fig.13 is summarized and confronted with predictions in Tab.9. The decay path length λ_{G4}, from a fit to the z distributions in Fig.13 of the form given in Eq.9,

agrees well with the expected value of $\gamma\beta c\tau$, obtained from PDG lifetimes and the given momenta.

Concerning the decay kinematics, we study the average of the neutrino-to-parent energy ratio $\langle E_\nu/E_{parent}\rangle$, as predicted by G4 and by the MiniBooNE redecay program `BooBeamNT`. `BooBeamNT` was written originally by Geoff Mills to boost the statistics on the neutrino fluxes at the MiniBooNE detector. This is accomplished by redecaying several times every neutrino-producing particle simulated in the beam Monte Carlo. The neutrino kinematics is derived analytically given the position, momentum, and polarization of the neutrino parents at decay. `BooBeamNT` is believed to correctly simulate the physics of all decay processes of relevance to MiniBooNE, and therefore we compare the `BooNEG4Beam` decay results to the `BooBeamNT` decay results. We make this comparison for ν_μ's and ν_e's separately.

As can be seen from the last two columns in Tab.9, ν_μ's from π^+ deciay are correctly simulated (note also the expected flat distribution in E_ν/E_{parent} in Fig.13). On the other hand, the neutrino kinematics for K^+, K^0_L, μ^+ decay is *not* in agreement between `BooNEG4Beam` and `BooBeamNT` [5]. As discussed in the GEANT4 "Physics reference Manual" [4] and in the `G4KL3DecayChannel` and `G4MuonDecayChannel`, these decays are expected to be wrong in GEANT4, because:

1. the correct Fermi's (V-A) theory is not applied to neutrinos, but only to the charged leptons;
2. the muon polarization is not taken into account.

For this reason, the predictions for ν_e fluxes in MiniBooNE should be generated via the (`BooNEG4Beam` + `BooBeamNT`) simulation chain, and not just by using `BooNEG4Beam`.

[5] For the μ^+ decays in `BooBeamNT`, we fixed the muon polarization in the muon rest frame to be $(0, 0, +1)$, where the z direction corresponds to the muon direction in the lab frame.

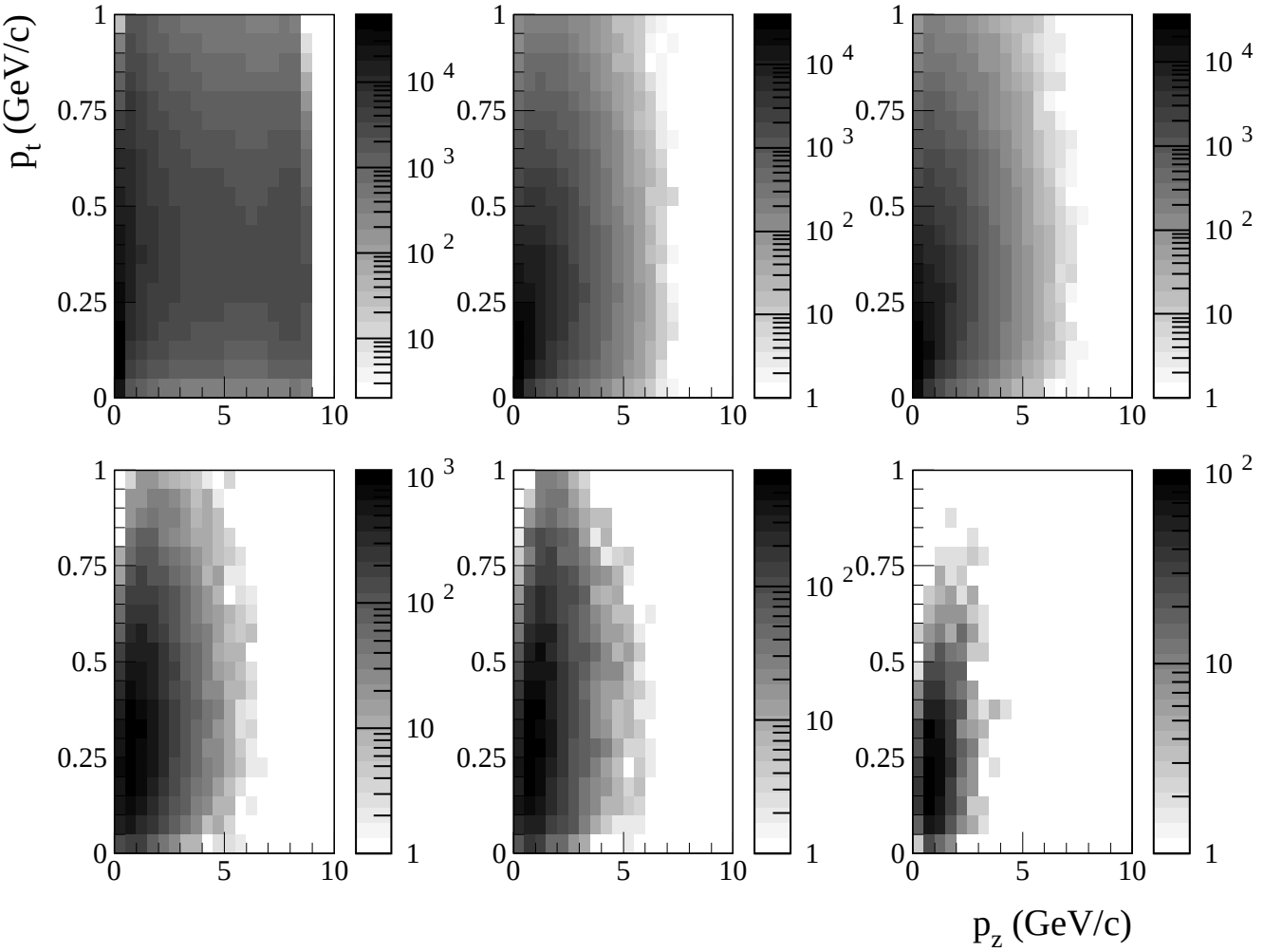

Figure 5: 2-dimensional histograms of the production momenta of secondary particles in inelastic collisions between primary protons and the MiniBooNE Be target. p_z is the longitudinal momentum with respect to the primary proton direction, p_t is the transverse momentum. Top left: secondary protons; tod middle: π^+; top right: π^-; bottom left: K^+, bottom middle: K^0_L; bottom right: K^-.

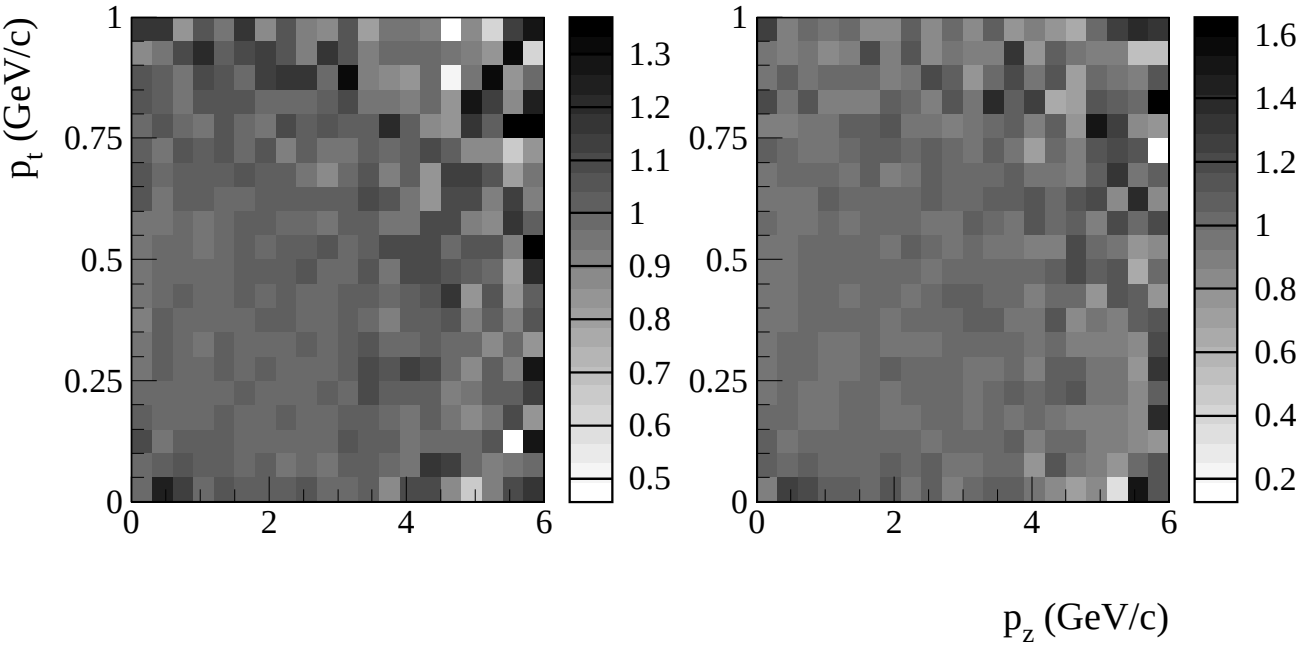

Figure 6: Cross-check on $\pi^{\pm}$ production multiplicity and kinematics, for inelastic collisions of primary protons in Be. Left plot: π^{+}; right plot: π^{-}. The plots show the number of events in (p_z, p_t) bins of the produced pion momentum, divided by the number of events in that bin given the number of inelastic collisions and final kinematics expected by the Sanford-Wang parametrization used in the simulation for the inclusive $\pi^{\pm}$ production. The 2D histograms are consistent with unity.

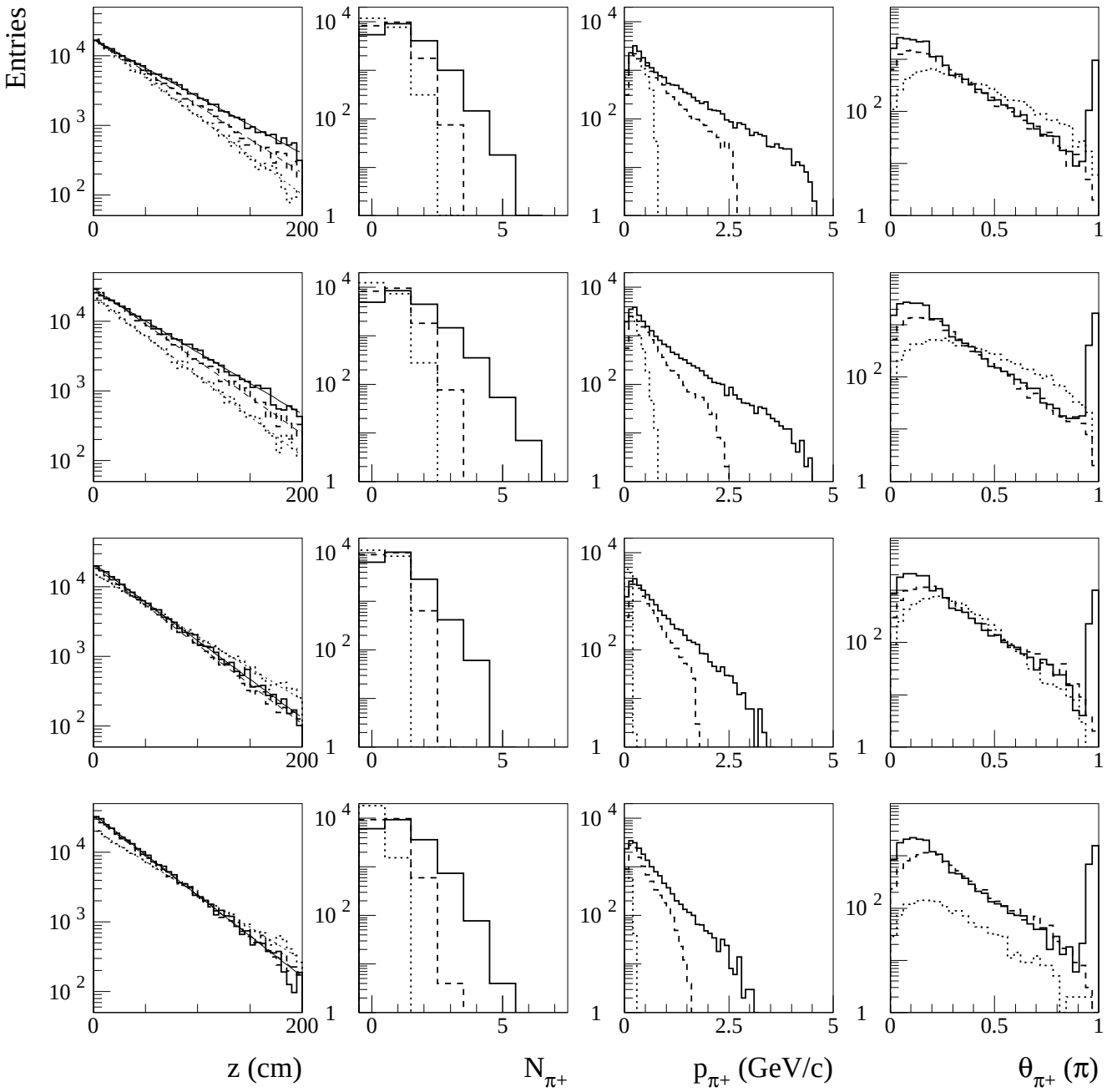

Figure 7: Cross-check on G4 inelastic processes for 1,3,5 GeV/c π^+'s and protons interacting in Beryllium and Aluminum. From left to right: distributions of the interaction position projected along the direction of the projectile, z; distribution of the final state π^+ multiplicity N_{π^+}, and momentum p_{π^+} and angle with respect to projectile direction θ_{π^+} for pions in the final state of the inelastic collisions. From top to bottom: π^+'s in Beryllium, π^+ in Aluminum, protons in Beryllium, protons in Aluminum. For each of the sixteen panels, the solid line is for 5 GeV/c projectiles, the dashed line for 3 GeV/c, the dotted line for 1 GeV/c.

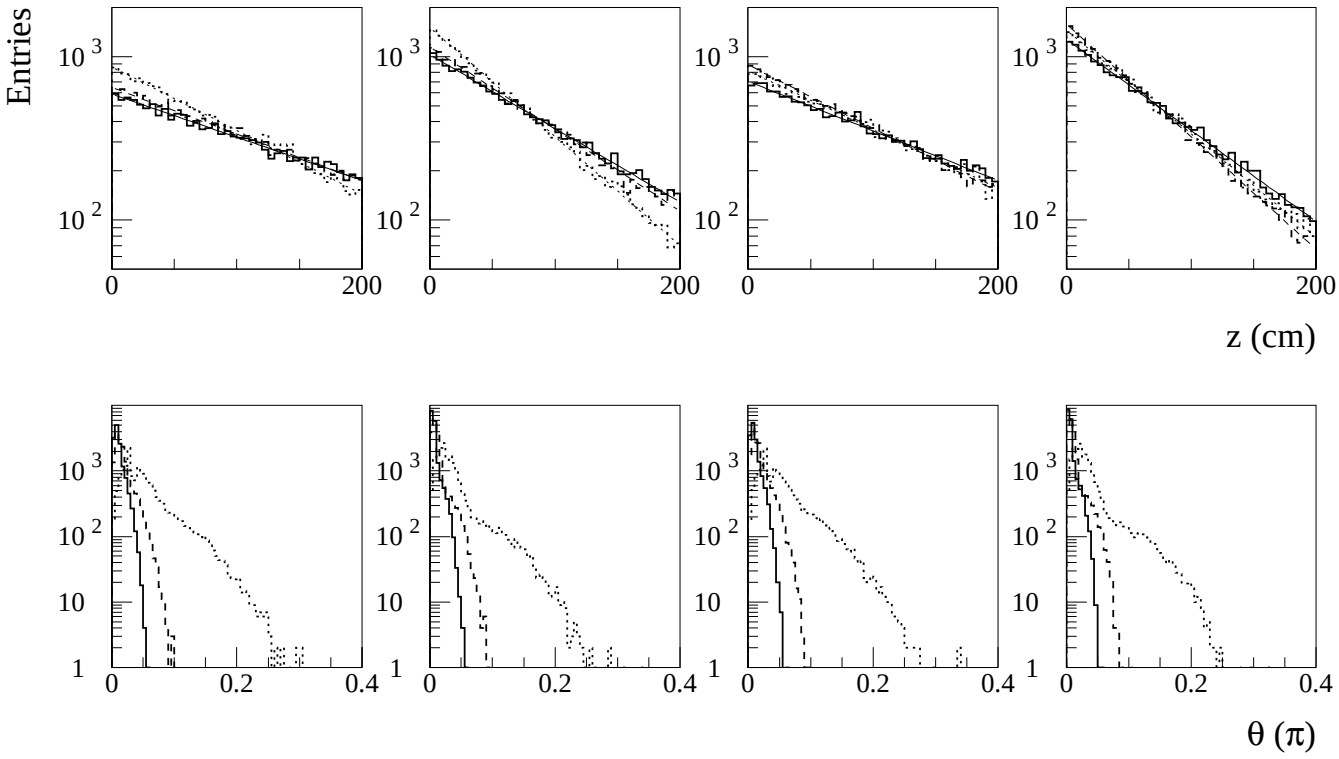

Figure 8: Cross-check on G4 elastic processes for 1, 3, 5 GeV/c π^+'sd and protons interacting in Beryllium and Aluminum. Top: distributions of the interaction position projected along the direction of the projectile, z; bottom: distribution of the π^+ angle with respect to projectile direction θ produced in the inelastic collision. From left to right: π^+'s in Beryllium, π^+ in Aluminum, protons in Beryllium, protons in Aluminum. For each of the eight panels, the solid line is for 5 GeV/c projectiles, the dashed line for 3 GeV/c, the dotted line for 1 GeV/c.

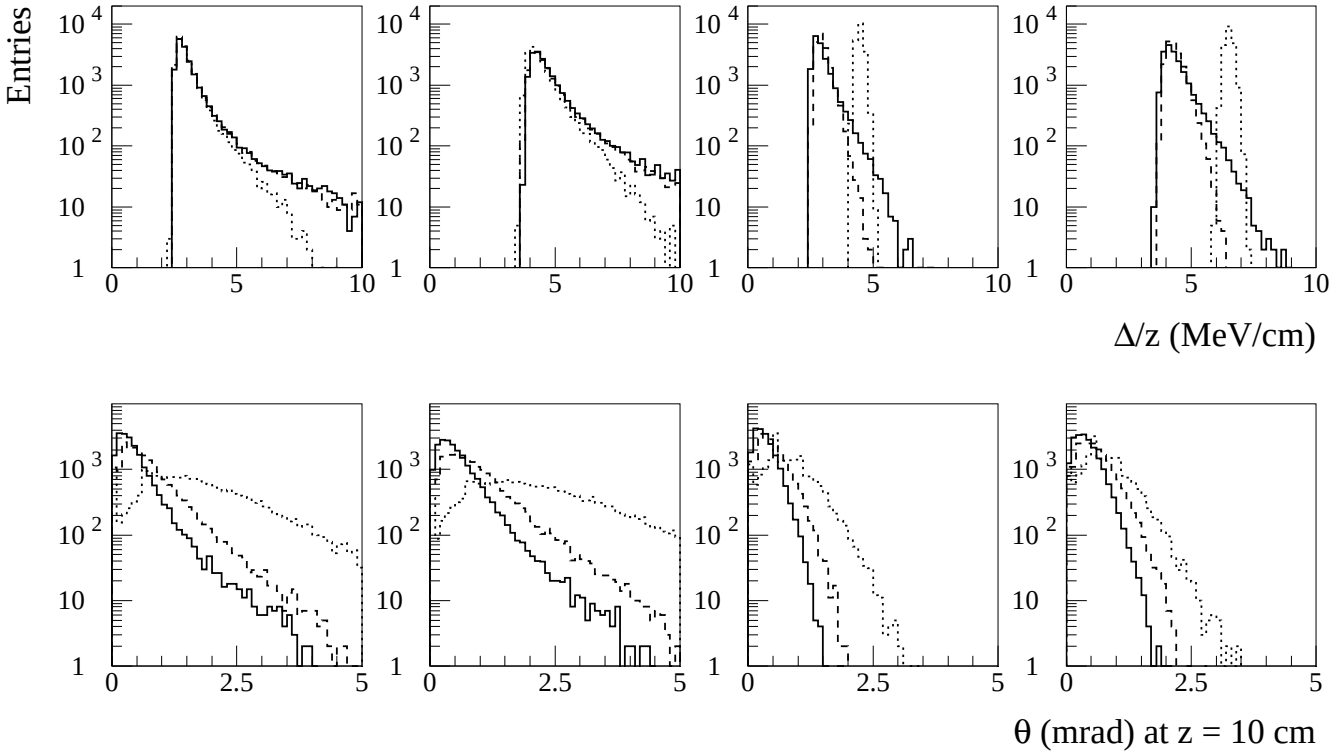

Figure 9: Energy loss results in GEANT4. Top plots: energy loss per unit material traversed, Δ/z; bottom plots: projectile deflection angle, θ, after traversing 10 cm of material. From left to right: π^+'s in Be, π^+'s in Al, protons in Be, protons in Al. For all eight panels, the solid line is for 5 GeV/c projectiles, the dashed line for 3 GeV/c, the dotted line for 1 GeV/c.

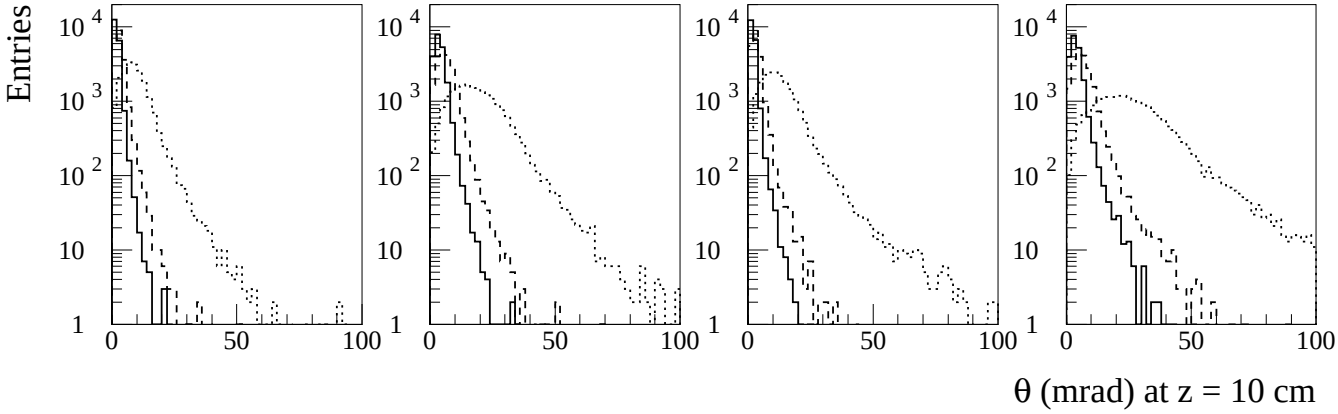

Figure 10: Deflection angles θ after traversing 10 cm of material, due to multiple Coulomb scattering. From left to right: π^+'s in Be, π^+'s in Al, protons in Be, protons in Al. For all plots, the solid histogram refers to 5 GeV/c projectiles, the dashed one to 3 GeV/c, the dotted one to 1 GeV/c.

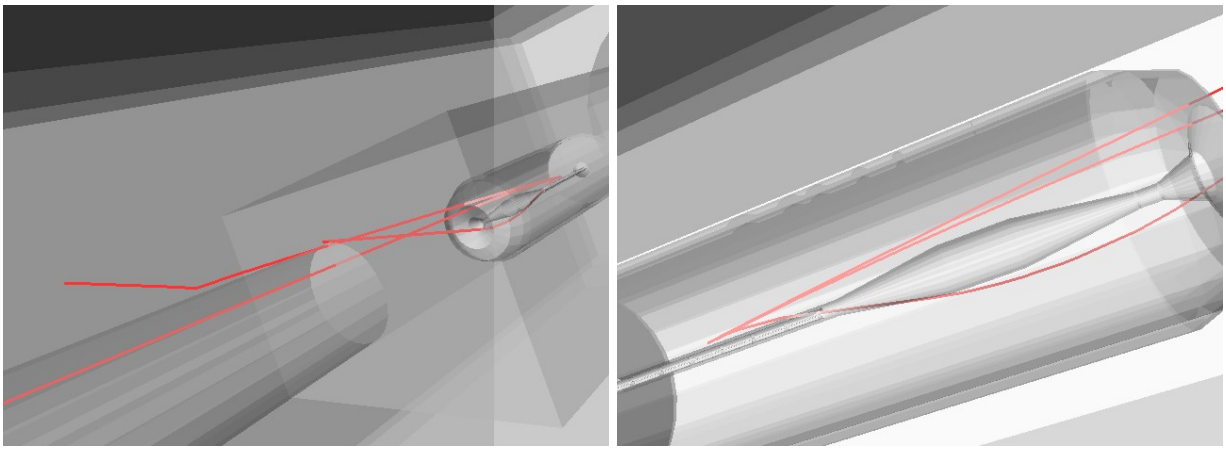

Figure 11: π^+ trajectories in the horn magnetic field. The three trajectories shown are for pions of 0.15, 2.0, and 5.0 GeV kinetic energy, produced near the horn axis at a 7° angle. The picture on the left shows only the 2.0 GeV trajectory reapching the downstream end of the cone collimator following the horn. The picture on the right shows the same tracks on a more detailed scale.

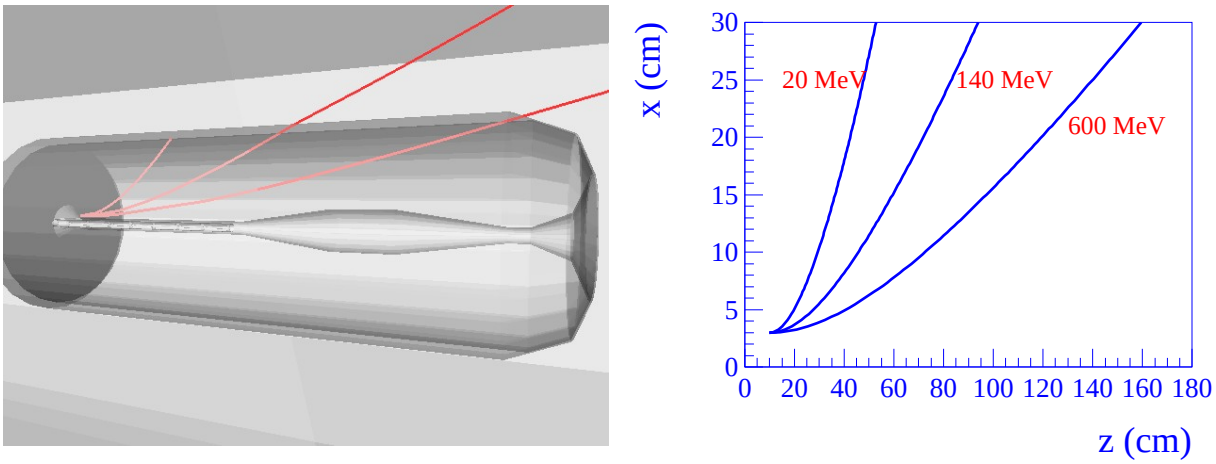

Figure 12: Trajectories in the horn magnetic field for 20, 140, and 600 MeV π^-'s, with initial conditions ($x_0 = 3$ cm, $z_0 = 10$ cm). Left: G4 trajectories, right: trajectories predicted by the CERNLIB routine `DRKNYS`.

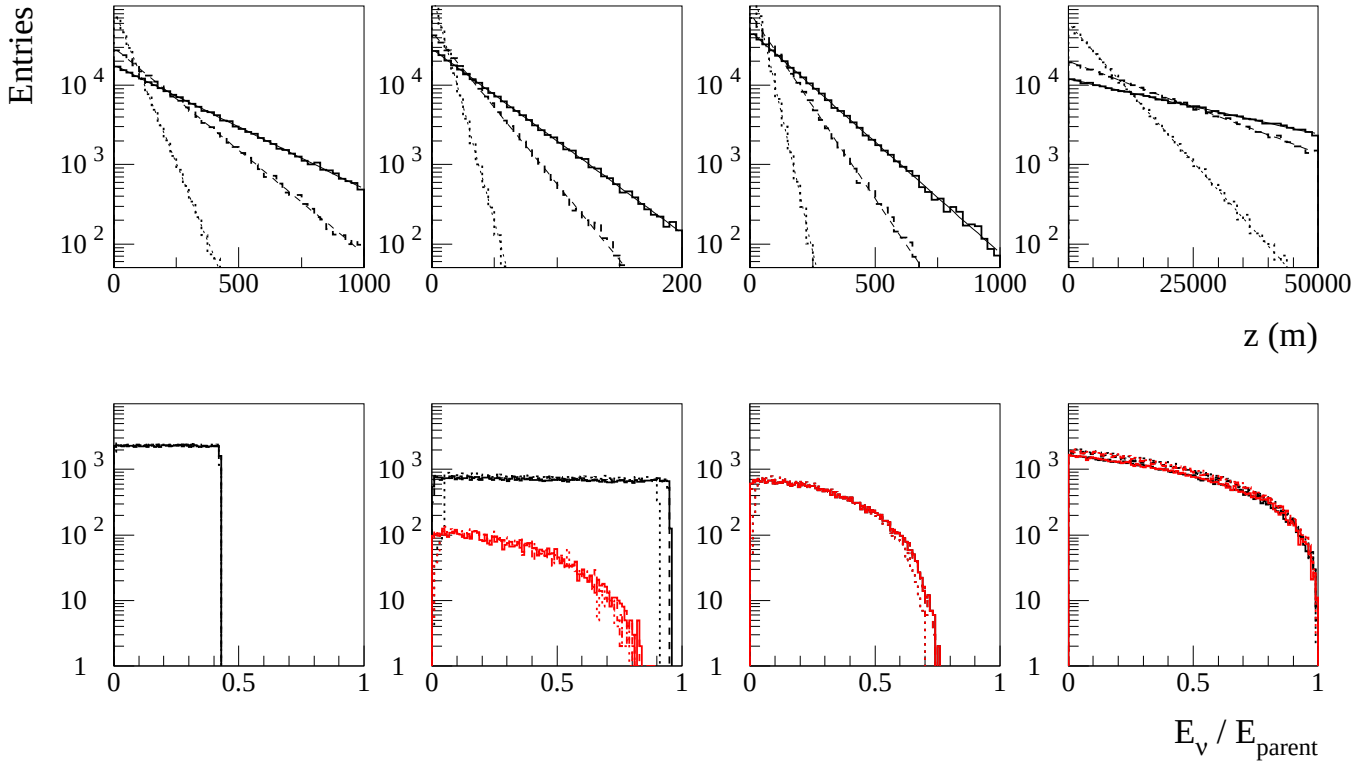

Figure 13: Cross-check on G4 decay processes. Top plots: z-distribution of particle decays in vacuum. Bottom plots: neutrino energy E_ν divided by the total energy of the neutrino producing parent, E_{parent}. From left to right: π^+, K^+, K^0_L, μ^+ decays. In all plots, the solid histograms are for 5 GeV/c parent tracks, the dashed ones for 3 GeV/c, the dotted ones for 1 GeV/c. In the bottom plots, the neutrino energies are shown separately for ν_μ's (black) and ν_e's (red).

5 Code validation 3: pion fluxes

In the previous Section we have discussed the validation of the physics processes of greatest relevance to MiniBooNE, as implemented in the GEANT4 kernel and in `BooNEG4Beam`, one by one; in this way, the simulation outcomes could often be confronted with simple analytical predictions. Now we wish to cross-check the combined effect of most of these physics processes, together with the MiniBooNE geometry description discussed in Section 3. In order to do this, we compare the `BooNEG4Beam` results with the ones obtained from an independent simulation program, `Model_B`.

5.1 `Model_B`: a brief description

`Model_B` is a MiniBooNE beam simulation program written by Mike Shaevitz. `Model_B` takes into account the most important effects shaping the MiniBooNE ν_μ flux. The program loops over the pion production location, pion momentum and angle at prooduction from p-Be interactions in the target, and maps this pion spectrum into a neutrino energy spectrum at the MiniBooNE detector. This is done by using numerical integration techniques that are more "transparent" to the user than the techniques used in a complicated Monte Carlo program such as GEANT4. The physics taken into account in `Model_B` is the following:

1. interaction length for p-Be inelastic interactions;
2. π^+ production in p-Be inelastic interactions, according to either a Sanford-Wang parametrization, or a MARS production identical to `BooNEG4Beam`. For the comparisons in this Section and in Section 6, we will use the `JAM` π^+ production model in both `Model_B` and `BooNEG4Beam`;
3. π^+ absorption in the Beryllium and Aluminum material traversed by the pion. The absorption lenght is modelled as the average of the inelastic and elastic interaction lengths as a function of material and pion momentum, obtained from `BooNEG4Beam`. The rationale for using this average is to include the effect of all inelastic reactions as well as that of elastic scattering at large angles, into absorption, since `Model_B` does not simulate the final state from pion interactions;
4. π^+ raytracing in the horn magnetic field. The trajectory is calculated numerically using the Runge-Kutta method in the CERNLIB routine `DRKNYS`, as described in the previous Section;
5. π^+ decay;
6. the phase space acceptance for the pion to decay into a ν_μ that hits the MiniBooNE detector.

In order to make sensible comparisons between the `Model_B` and `BooNEG4Beam` results, we have simplified the `BooNEG4Beam` physics as follows:

1. used a "pencil beam" description for the primary protons, that is zero transverse spot size on target and no angular divergence;
2. in the primary p-Be inelastic interaction modelled by `BooNEpBeInteraction`, only π^+'s are produced, and no π^-'s, $K^\pm$'s, or K^0_L's;
3. turned off ionisation and multiple Coulomb scattering for all particles.

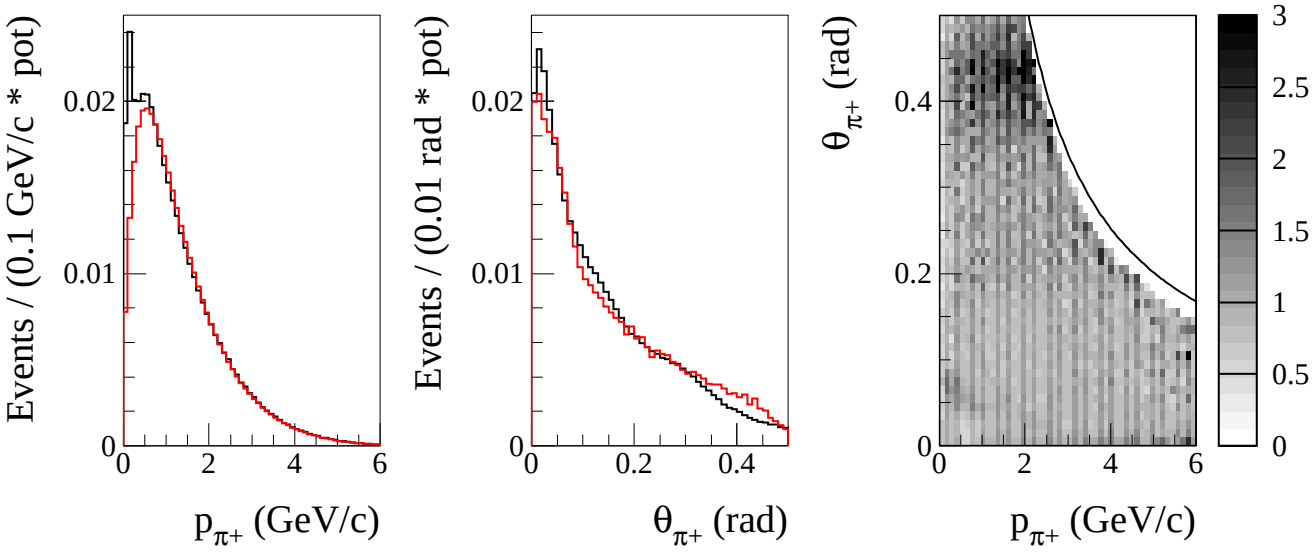

Figure 14: `Model_B`/`BooNEG4Beam` comparisons of pion fluxes after the horn. The pion momentum p_{π^+} and angle θ_{π^+} distributions are shown in black for `BooNEG4Beam`, in red for `Model_B`. The right scatter plot in the $(p_{\pi^+}, \theta_{\pi^+})$ plane shows the ratio between the `Model_B` and `BooNEG4Beam` yields. The solid curve is for $p_t = 1$ GeV/c, the maximum p_t value sampled in `BooNEG4Beam`.

Position	$N_{\pi+}$/pot		$\langle p_{\pi+} \rangle$ (GeV/c)		$\theta_{\pi+}$ (rad)	
	Model_B	G4	Model_B	G4	Model_B	G4
After horn	0.357	0.383	1.31	1.24	0.153	0.141
After collimator	0.117	0.134	1.53	1.46	0.035	0.045

Table 10: Summary on `Model_B`/`BooNEG4Beam` comparisons of pion fluxes, after the horn and after the collimator. The pion fluxes per proton on target, the average pion momentum and angle are given at both planes, for both `Model_B` and `BooNEG4Beam`.

In this section, we compare the pion fluxes at different locations along the MiniBooNE beamline from `Model_B` and this simplified version of `BooNEG4Beam`; the neutrino flux comparison is discussed in the next Section. The `Model_B` code used to make these comparisons was kindly provided by Mike Shaevitz.

5.2 Pion fluxes after the horn

A `Model_B`/`BooNEG4Beam` comparison of pion fluxes after the horn, at $z = 200$ cm where $z = 0$ indicates the upstream face of the horn, is useful to check (mostly) pion production and pion deflection in the horn magnetic field. Number of pions, and the distributions of pion momenta and angles are shown in Fig.14; the mean values for these quantities are given in the "After horn" row in Tab.10

The agreement is good, at the few % level, both in terms of overall number of pions and in the

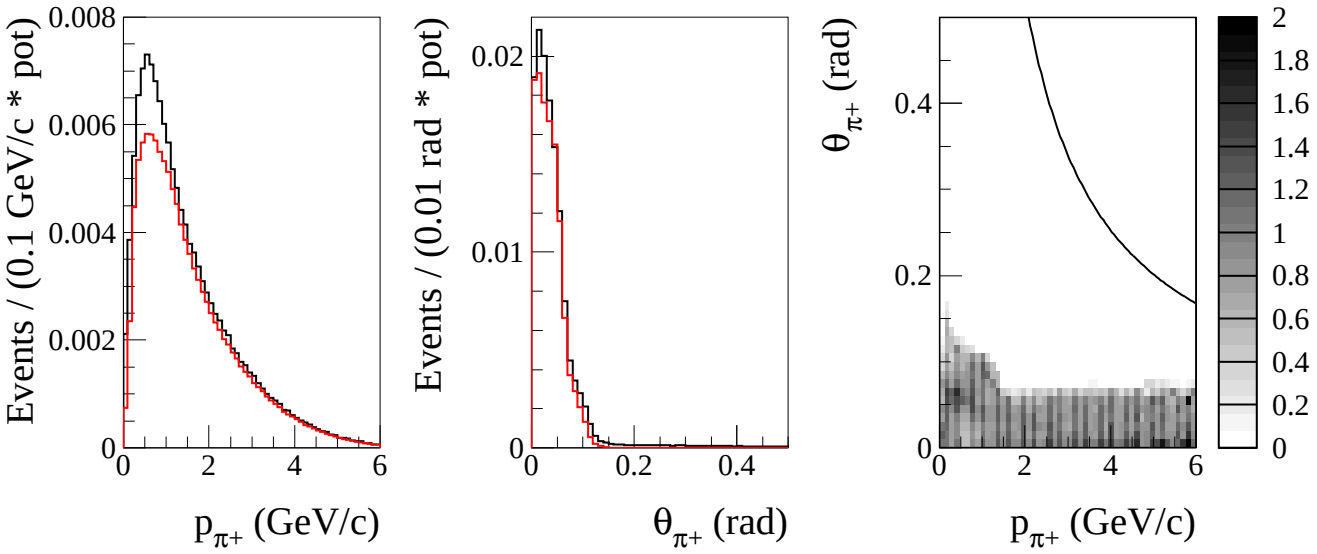

Figure 15: `Model_B`/`BooNEG4Beam` comparisons of pion fluxes after the collimator. The pion momentum p_{π^+} and angle θ_{π^+} distributions are shown in black for `BooNEG4Beam`, in red for `Model_B`. The right scatter plot in the $(p_{\pi^+}, \theta_{\pi^+})$ plane shows the ratio between the `Model_B` and `BooNEG4Beam` yields. The solid curve is for $p_t = 1$ GeV/c, the maximum p_t value sampled in `BooNEG4Beam`.

pion momentum distributions $(p_{\pi^+}, \theta_{\pi^+})$ recorded at a plane after the horn. Minor discrepancies can be seen at low pion momenta, where `BooNEG4Beam` predicts more pions, and at large pion angles. Those might be explained by the fact that `BooNEG4Beam` simulates outgoing pions in pion inelastic and elastic interactions, while `Model_B` does not. On the other hand, pions with low momentum and large angles after the horn are not expected to contribute much to the MiniBooNE ν_μ flux.

5.3 Pion fluxes after the collimator

Pion yields and momentum distributions from `BooNEG4Beam` and `Model_B` in a plane downstream of the cone collimator are compared in Fig.15. The plane is defined as the $z = 560$ cm plane in global coordinates. The mtivation for type of check is similar to the one after the horn, but places more emphasis on the pions that ultimately matter to MiniBooNE.

The comparison of the distributions in Fig.15 is summarized in the "After collimator" row in Tab.10. The agreement is a little poorer at this z location, in particular for < 1.5 GeV/c pion momenta, where `BooNEG4Beam` predicts significantly more pions. Pion yields, pion average momenta, and pion average angles after the collimator agree within $\sim$20% between `BooNEG4Beam` and `Model_B`.

The comparisons shown in this Section, while more difficult to interpret than the ones given in Sections 3 and 4, show that the `BooNEG4Beam` predictions can be reproduced reasonably well by an independent and esier-to-understand program such as `Model_B`, indicating that most of the relevant physics affecting the pion fluxes can be identified and understood, and that no major deficiencies are present in `BooNEG4Beam`.

6 Code validation 4 and results: neutrino fluxes at the MiniBooNE detector

The final results of a MiniBooNE Monte Carlo, and the only ones that ultimately matter, are the predictions for the neutrino fluxes at the MiniBooNE detector. In this Section we discuss:

1. comparisons on the ν_μ flux between `Model_B` and a simplified version of `BooNEG4Beam`;
2. comparisons on the fluxes of all neutrino flavors between the GEANT3.21 beam Monte Carlo `BooBeamMC` and `BooNEG4Beam`, for both a GFLUKA and MARS production;
3. results on the fluxes of all neutrino flavors from a variety of models in `BooNEG4Beam`, including the currently used `JAM` model.

Large pion decay statistics is needed in order to produce smooth distributions as a function of neutrino energy in the small solid angle subtended by the MiniBooNE detector; for this reason, the results from the `BooBeamMC` and `BooNEG4Beam` Monte Carlo programs shown in this Section are obtained by redecaying all neutrino-producing parent particles 1000 times via the `BooBeamNT` decay simulator program. All fluxes are obtained considering neutrinos crossing a 6.1 m radius circle centered on the beam axis and located 541 m downstream of the target.

6.1 Comparison of G4/`Model_B` neutrino fluxes at the detector

Fig.16 shows the ν_μ fluxes predicted by `Model_B` and the simplified version of `BooNEG4Beam` (see Section 5 for details on `Model_B` and the meaning of "simplified" in the previous sentence).

Apart from the peak in the lowest-energy bin of the `BooNEG4Beam` ν_μ flux (which disappears by adding all physics processes, in particular ionisation and multiple Coulomb scattering), there are some other differences in the predictions from the two programs: `Model_B` predicts a flux that is larger and more energetic than `BooNEG4Beam`. However, the discrepancy between the two programs is limited to 5-10%, as summarized in Tab.11.

Simulation	ϕ_{ν_μ} $(10^{-10}/(cm^2 \cdot \text{pot}))$	$\langle E_{\nu_\mu}\rangle_{\phi_\nu}$ (GeV)	$\langle p_{\pi+}\rangle_{\phi_\nu}$ (GeV/c)	$\langle \theta_{\pi+}\rangle_{\phi_\nu}$ (rad)
`Model_B`	4.82	0.844	2.25	0.097
`BooNEG4Beam`	4.72	0.759	2.10	0.104

Table 11: Summary on `Model_B/BooNEG4beam` comparisons of the ν_μ flux at the MiniBooNE detector. The overall ν_μ flux ϕ_{ν_μ}, as well as the avearge neutrino energy ($\langle E_{\nu_\mu}\rangle_{\phi_\nu}$), pion production momentum ($\langle p_{\pi^+}\rangle_{\phi_\nu}$) and production angle ($\langle \theta_{\pi^+}\rangle_{\phi_\nu}$) for pions giving neutrinos in MiniBooNE are given for both `Model_B` and `BooNEG4Beam`. The average values are to be intended as averages over the ν_μ flux distribution.

In Fig.17 and Tab.11 we also show the pion momentum and angle distributions at pion production, for pions producing neutrinos in the MiniBooNE detector. The pion momentum comparison show the same trend as the neutrino energy comparison, while the pion production angle for pions producing MiniBooNE neutrinos is slightly smaller in `Model_B` than it is in `BooNEG4Beam`. The level

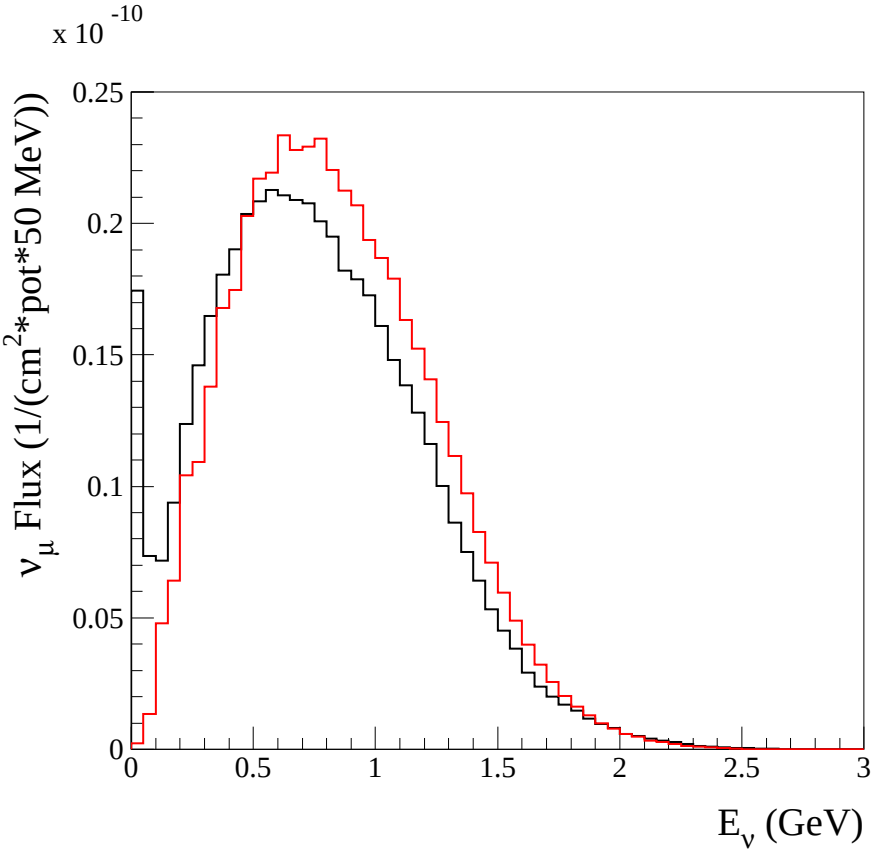

Figure 16: ν_μ flux as a function of neutrino energy E_ν predicted by the same `JAM` production model in a simplified version of `BooNEG4Beam` (black) and in `Model_B` (red).

of agreement is at the same level as for the neutrino energy distribution.

In Fig.,17, we also show the curve corresponding to $p_t = 1$ GeV/c in the $(p_{\pi^+}, \theta_{\pi^+})$ plane. As explained in Section 4, in `BooNEG4Beam` the pion production is parametrized in terms of longitudinal and transverse momentum: Fig.17 shows that the upper limit of 1 GeV/c used for the p_t sampling is sufficient, as only a negligibly small fraction of pions of higher transverse momenta produce neutrinos in the MiniBooNE detector. This conclusion holds true for other mesons as well.

6.2 Comparison of G4/G3 neutrino fluxes at the detector

Two of the production physics models present in `BooNEG4Beam` are also present in the GEANT3.21 beam monte Carlo, `BooBeamMC`: those are the GFLUKA and MARS production models. `BoobeamMC` is the beam Monte Carlo program used to generate the MiniBooNE neutrino fluxes prior to `2003-08-15` release; for more details on `BoobeamMC`, see [11]. We can therefore make a direct comparison on the neutrino distributions predicted by these two different programs as well. Both simulations were done with default settings, including nonzero primary beam spot size and divergence, production of particles other than π^+'s in p-Be interactions, ionisation, and multiple

Production Model	Neutrino Type	ϕ_ν $((cm^2 \cdot \text{pot})^{-1})$		$\langle E \rangle_{\phi_\nu}$ (GeV)	
		G3	G4	G3	G4
MARS	ν_e	$1.27 \cdot 10^{-12}$	$2.04 \cdot 10^{-12}$	0.713	0.851
MARS	$\bar{\nu}_e$	$2.16 \cdot 10^{-13}$	$2.94 \cdot 10^{-13}$	0.670	0.983
MARS	ν_μ	$3.03 \cdot 10^{-10}$	$4.18 \cdot 10^{-10}$	0.725	0.724
MARS	$\bar{\nu}_\mu$	$1.48 \cdot 10^{-11}$	$2.72 \cdot 10^{-11}$	0.390	0.436
GFLUKA	ν_e	$2.81 \cdot 10^{-12}$	$2.43 \cdot 10^{-12}$	1.010	1.001
GFLUKA	$\bar{\nu}_e$	$3.40 \cdot 10^{-13}$	$2.77 \cdot 10^{-13}$	1.131	1.108
GFLUKA	ν_μ	$8.29 \cdot 10^{-10}$	$7.47 \cdot 10^{-10}$	0.975	0.976
GFLUKA	$\bar{\nu}_\mu$	$5.56 \cdot 10^{-11}$	$4.52 \cdot 10^{-11}$	0.856	0.858

Table 12: G3/G4 comparisons on the ν_e, $\bar{\nu}_e$, ν_μ, $\bar{\nu}_\mu$ fluxes at the MiniBooNE detector, for both the MARS and GFLUKA production models. The comparison is given in terms of overall fluxes ϕ_ν and neutrino energies averaged over the flux distribution, $\langle E \rangle_{\phi_\nu}$.

Coulomb scattering, effects which were turned off in the `Model_B/BooNEG4Beam` comparisons. Moreover, we can compare not only the ν_μ fluxes, but the fluxes for other neutrino flavors as well. We can compare the results from the two simulations to the extent that the geometry specifications are identical and the primary mechanisms for producing mesons in p-Be interactions should be very similar [6]; however, no effort has been made to match other physics models between `BooNEG4Beam` and `BooBeamMC`, since this would be very difficult on a practical level. The GEANT3 distributions are kindly provided by Terry Hart.

Fig.18 shows the ν_e,$\bar{\nu}_e$,ν_μ,$\bar{\nu}_\mu$ fluxes as a function of neutrino energy for both the MARS (top) and GFLUKA (bottom) production models, overlaying the `BooNEG4Beam` predictions to the `BooBeamMC` ones. Tab.12 summarizes the information contained in Fig.18 by comparing the overall fluxes and the average energies weighted by the flux distributions.

Concerning the energy shape, the agreement between the G3 and G4 Monte Carlo programs is excellent, at the sub-percent level, on the ν_μ energy shape, for both the MARS and GFLUKA models. The GFLUKA ν_e energy shapes are also in very good agreement, while the ν_e average energy predicted by G4/MARS is about 20than the G3/MARS one.

Concerning the overall flux normalizations, the agreement between the G3 and G4 simulations gets worse. In particular, the G4 MARS fluxes are higher than the G3 MARS fluxes by 60% for ν_e's and 38% for ν_μ's [7]. On the contrary, the G3 GFLUKA fluxes are higher than the G4 GFLUKA fluxes by 16% for ν_e's and 11% for ν_μ's.

[6] Note, however, that the MARS comparison might not be entirely fair, as the G3 Monte Carlo used slightly older MARS cross-sections than the G4 Monte Carlo. It is not known how much these cross-sections might have changed.

[7] The G3/G4 discrepancy on the overall MARS ν_μ flux normalization is reduced to 12% by considering the G3/MARS value given in [11], corresponding to $3.72 \cdot 10^{-10}$ $(cm^2 \cdot pot)^{-1}$.

Model	ϕ $((cm^2 \cdot \text{pot})^{-1})$				$\langle E_\nu \rangle_\phi$ (GeV)			
	ν_e	$\bar{\nu}_e$	ν_μ	$\bar{\nu}_\mu$	ν_e	$\bar{\nu}_e$	ν_μ	$\bar{\nu}_\mu$
GFLUKA	$2.43 \cdot 10^{-12}$	$2.77 \cdot 10^{-13}$	$7.47 \cdot 10^{-10}$	$4.52 \cdot 10^{-11}$	1.001	1.108	0.976	0.858
MARS	$2.04 \cdot 10^{-12}$	$2.94 \cdot 10^{-13}$	$4.18 \cdot 10^{-10}$	$2.72 \cdot 10^{-11}$	0.851	0.983	0.724	0.436
CHO	$1.93 \cdot 10^{-12}$	$2.85 \cdot 10^{-13}$	$4.54 \cdot 10^{-10}$	$2.82 \cdot 10^{-11}$	0.879	0.919	0.800	0.530
JAM	$1.89 \cdot 10^{-12}$	$2.79 \cdot 10^{-13}$	$4.16 \cdot 10^{-10}$	$2.88 \cdot 10^{-11}$	0.870	0.909	0.769	0.540

Table 13: Summary on `BooNEG4Beam` ν_e, $\bar{\nu}_e$, ν_μ, $\bar{\nu}_\mu$ fluxes at MiniBooNE, for four different production models. The table gives the overall fluxes and the average neutrino energies.

6.3 G4 results on neutrino fluxes

We conclude this Section by comparing various neutrino flux predictions obtained via the `BooNEG4Beam` beam Monte Carlo only, for a 50 m long decay region and in neutrino running mode. We give the results for ν_e, $\bar{\nu}_e$, ν_μ, $\bar{\nu}_\mu$ fluxes obtained from four `BooNEG4Beam` models differing in the particle production in p-Be interactions:

1. `GFLUKA`
2. `MARS`
3. `ZGS`
4. `JAM`

Those models were discussed in Section 4. Fig.19 shows the neutrino energy distributions for all neutrino flavors and for the four production physics models listed above, predicted by `BooNEG4Beam` with default settings. Tab.13 summarizes the neutrino fluxes and average neutrino energies, obtained from Fig.19.

While the overall ν_e fluxes are similar among the four production models (partly by construction, see Tab.1), the ν_μ fluxes vary greatly. The `JAM` predictions for the fluxes are $1.89 \cdot 10^{-12}$ $(cm^2 \cdot pot)^{-1}$ for the ν_e's, $4.16 \cdot 10^{-10}$ $(cm^2 \cdot pot)^{-1}$ for the ν_μ's, the ratio being 0.45%.

The predictions for different production models differ less in the neutrino energy shape than in the overall normalization; nevertheless, significant differences are still present. In general, models with higher neutrino fluxes tend to have harder spectra. For `JAM`, the neutrino energies averaged over the flux distributions (and not over the flux times cross-section) are 0.87 and 0.77 GeV for ν_e's and ν_μ's, respectively.

Finally, in Tab.14, we show the fraction of ν_e and ν_μ fluxes subdivided per neutrino parent, for the `JAM`/`BooNEG4Beam` simulation. This model predicts that about half of the ν_e flux is due to muon decays, and about 40$ is due to charged kaon decays; on the other hand, as also shown in Tab.14, ν_e's from kaon decays are of much higher energy than ν_e's from muon decays. Almost all of ν_μ's are instead produced in pion decays (97.5%).

Neutrino	Parent	Flux fraction per parent (%)	Average neutrino energy per parent (GeV)
ν_e	μ^+	49.1	0.59
	π^+	0.0	n.a.
	K^0_L	11.2	1.08
	K^+	39.7	1.32
ν_μ	μ^+	0.0	0.32
	π^+	97.5	0.75
	K^0_L	0.0	1.14
	K^+	2.4	2.04

Table 14: Flux fractions and average neutrino energies for ν_e's and ν_μ's, from the `JAM/BooNEG4Beam` simulation, subdivided per neutrino parent. Note that the $\pi^+ \rightarrow e^+\nu_e$ decay is not currently implemented in `BooNEG4Beam`.

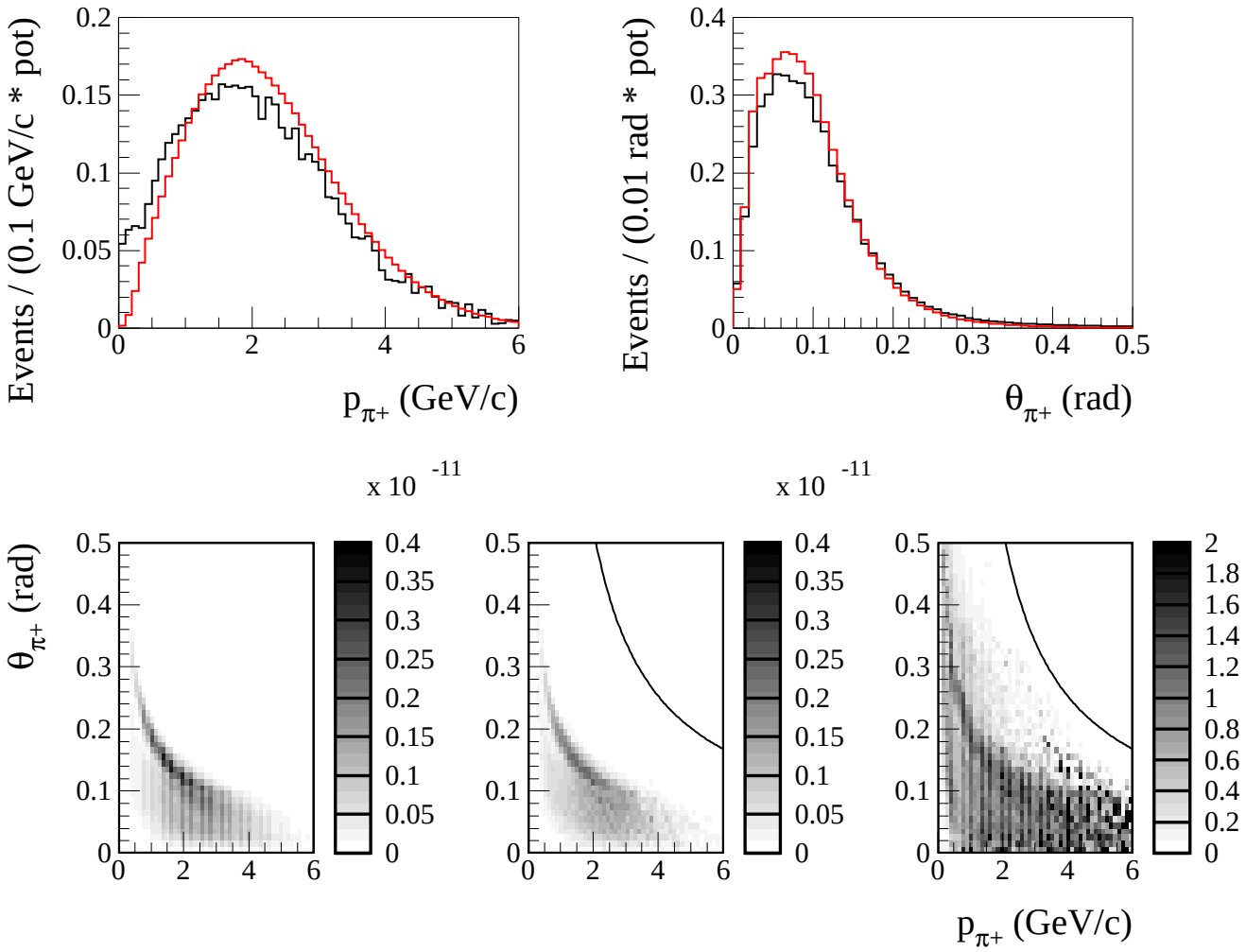

Figure 17: `Model_B`/`BooNEG4Beam` comparisons on the pion momentum (p_{π^+}) and angle (θ_{π^+}) at production, for pions giving neutrinos in the MiniBooNE detector. The top two plots show the `BooNEG4Beam` histograms in black, the `Model_B` histograms in red. The bottom left and middle plots show the same $p_{\pi^+}, \theta_{\pi^+}$ quantities in a scatter plot, for `Model_B` and `BooNEG4Beam`, respectively. The bottom right plot shows the ratio of the `Model_B` yields divided by the `BooNEG4Beam` yields in the $(p_{\pi^+}, \theta_{\pi^+})$ plane. The black curve in the bottom middle and right plots shows the $p_t = 1$ GeV/c curve.

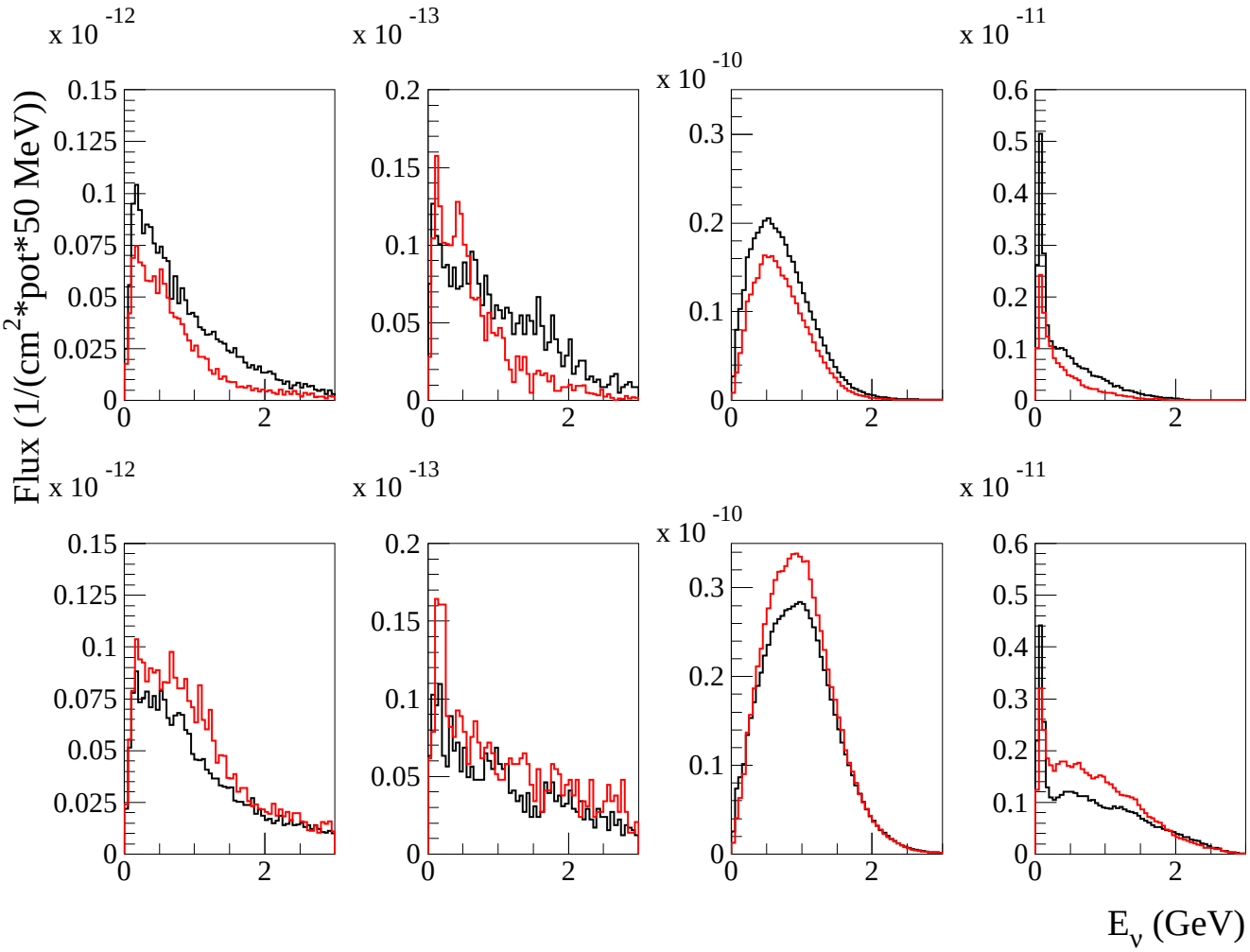

Figure 18: Comparisons of the neutrino fluxes at the MiniBooNE detector as a function of neutrino energy E_ν between the G3 beam Monte Carlo `BooBeamMC` (red) and the G4 one, `BooNEG4Beam` (black). From left to right: ν_e, $\bar{\nu}_e$, ν_μ, $\bar{\nu}_\mu$ fluxes. The top plots are for the MARS production model, the bottom ones for the GFLUKA model.

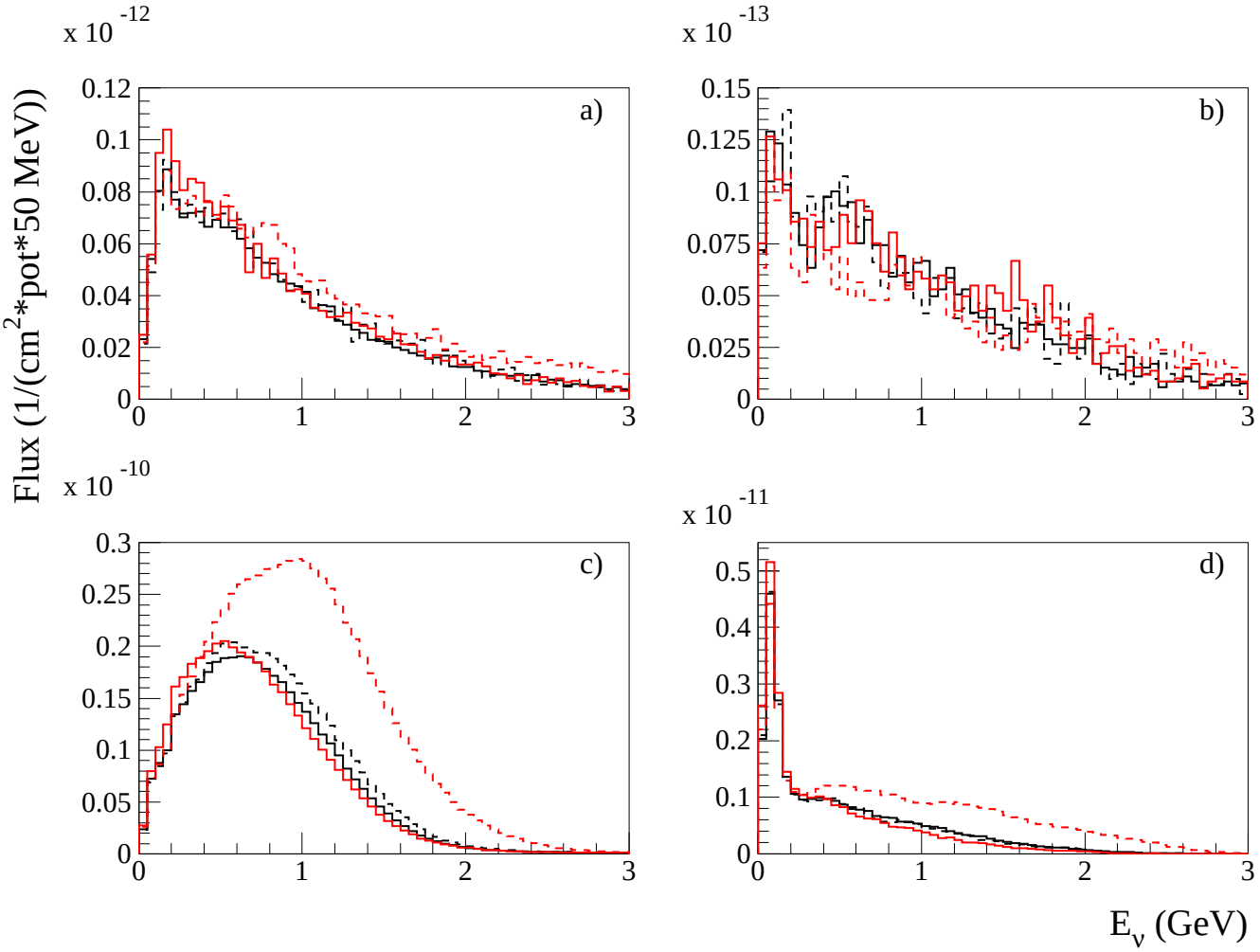

Figure 19: Neutrino fluxes at the MiniBooNE detector as a function of neutrino energy E_ν, as predicted by various production models, from the GEANT4 beam Monte Carlo. The four panels are for: a) ν_e, b) $\bar{\nu}_e$, c) ν_μ, d) $\bar{\nu}_\mu$. On each panel, there are four histograms, corresponding to four different production models for p-Be inelastic interactions: black solid is `JAM`, black dashed is `ZGS`, red solid is `MARS`, red dashed is `GFLUKA`. See text for details on these four models.

7 Conclusions

In this technical note, a GEANT4-based beam Monte Carlo for MiniBooNE, `BooNEG4Beam`, is described in detail. The scope of the simulation program is to predict the ν_e, $\bar{\nu}_e$, ν_μ, $\bar{\nu}_\mu$ fluxes at the MiniBooNE detector. The most important design requirement is to provide a flexible and transparent physics interface to the user, in particular concerning the physics of particle production in proton interactions in the MiniBooNE Beryllium target, because the uncertainties in the hadronic production models represent the dominant source of uncertainties in the MiniBooNE neutrino fluxes. The concrete implementation of this design requirement (and other requirements) as a GEANT4 application is explained and motivated.

Over the past two years, extensive validation of the code has been done, in conjunction with the code development. A number of cross-checks were presented in this note, aiming to quantify the accuracy of the simulation at the basic level of geometry specification, event generation, and description of the individual physics processes of relevance to MiniBooNE. A more complete (and complex) code validation has also been described, by comparing the `BooNEG4Beam` results to two independent simulation programs, `Model_B` and `BooBeamMC`, using as consistent as possible physics inputs to the different programs. These comparisons generally yielded satisfactory results.

Finally, a summary on the ν_e, $\bar{\nu}_e$, ν_μ, $\bar{\nu}_\mu$ fluxes at the MiniBooNE detector, as currently predicted by various hadronic physics options in `BooNEG4Beam`, is given. This summary includes results on the neutrino flux prediction currently used in MiniBooNE, which is given by the `JAM` production model.

8 Acknowledgments

I would like to thank Steve Brice, Daniel Elvira, Chris Green, Jeff Kallenbach, Geoff Mills, Byron Roe, Bill Seligman, Panagiotis Spentzouris, and Eric Zimmerman for useful suggestions on how to structure the code, and for building and maintaining the GEANT4 toolkit at FNAL. I would also like to thank Terry Hart, Jocelyn Monroe, Mike Shaevitz, and Sam Zeller for helping me in the code validation process.

References

[1] M. Sung and H. White, "New Method for Neutrino Flux Measurement for BooNE", BooNE Technical Note # 88.

[2] S. H. Ahn *et al.* [K2K Collaboration], Phys. Lett. B **511**, 178 (2001) [arXiv:hep-ex/0103001].

[3] P. Astier *et al.* [NOMAD Collaboration], Phys. Lett. B **570**, 19 (2003) [arXiv:hep-ex/0306037].

[4] `http://wwwasd.web.cern.ch/wwwasd/geant4/G4UsersDocuments/Overview/html/`

[5] `http://www-boone.fnal.gov/software_and_analysis/beam_group/software/links/geant4/`

[6] B. Roe, "Some Thoughts on the Beam Monte Carlo", `http://www-boone.fnal.gov/memos/thoughts_on_MC.ps.gz`

[7] `http://www-boone.fnal.gov/software_and_analysis/boone-condor/`

[8] Y. Cho *et al.*, Phys. Rev. D **4**, 1967 (1971).

[9] J. Monroe, WIN2003 plot memos, "Sanford-Wang Fit to Pion Production Data", `http://www-boone.fnal.gov/memos/swfit.ps`

[10] Particle Data Group website, `http://pdg.lbl.gov/`

[11] J, Monroe, "Comparison of MARS vs. GEANT3 Simulated Neutrino Flux in the MiniBooNE Detector Acceptance", BooNE Technical Note # 56